

Linkages between nitrogen cycling, nitrogen isotopes and environmental properties in paleo-lake basins

Liuwen Xia¹, Jian Cao^{1*}, Eva E. Stüeken^{2*}, Wenxuan Hu¹, Dongming Zhi³

1. MOE Key Laboratory of Surficial Geochemistry, School of Earth Sciences and Engineering, Nanjing University, Nanjing, Jiangsu 210023, China

2. School of Earth & Environmental Sciences, University of St Andrews, St Andrews, Fife, KY16 9AL Scotland, UK

3 PetroChina Xinjiang Oilfield Company, Karamay, Xinjiang 843000, China

Published in *GSA Bulletin*, <https://doi.org/10.1130/B36290.1>

Abstract

The linkages between nitrogen cycling, nitrogen isotopes, and environmental properties are fundamental for reconstructing nitrogen biogeochemistry. While the impact of ocean redox changes on nitrogen isotopes is relatively well understood, it is poorly known how nitrogen responds to changes in pH and salinity. To fill the knowledge gap, we explore the effects of these environmental parameters using a well-controlled set of samples from Carboniferous–Paleogene lake sediments in China. Our results show that the threshold of 10–12‰ in $\delta^{15}\text{N}$ works to distinguish alkaline (pH > 9) from circum-neutral conditions. Elevated Mo levels in the alkaline samples support the idea of NH_3 volatilization from a reducing water column in an alkaline setting. For non-alkaline lakes, $\delta^{15}\text{N}$ values tend to be higher (up to +10‰) in more saline, anoxic settings, which is attributed to either the expansion of stagnant anoxic waters spurring water-column denitrification or a shift from plant-based towards more microbially-dominated ecosystems or both. Our results imply that salinity-induced redox stratification and basicity can alter nitrogen biogeochemical cycling beyond what is shown by the marine nitrogen isotope record alone. This will result in an improved understanding of the dynamic controls of $\delta^{15}\text{N}$ in sediments and lead to better biogeochemical interpretations of paleo-environmental conditions from unknown environmental settings on Earth and beyond Earth.

Keywords: biogeochemical nitrogen cycle; basicity; saline lacustrine basin; alkaline lake; salinity; redox state

1. Introduction

Nitrogen is an essential nutrient for all organisms and plays a key role in the Earth system (Dos Santos et al., 2012). It is therefore crucial to optimize the $\delta^{15}\text{N}$ proxy for reconstructing nitrogen cycling through Earth history. In modern marine environments with

relatively stable salinity and pH, the biological nitrogen cycle is mainly controlled by the relative changes of nitrogen fixation and incomplete denitrification, which is closely related to the size of oxygen minimum zones and hence redox (Sigman et al., 2009). The main form of nitrogen in oxic modern oceans is NO_3^- , and the mean $\delta^{15}\text{N}$ value is about +5‰ with local variability of a few permil. However, potential effects of salinity and pH on $\delta^{15}\text{N}$ are not well constrained as seawater has a relatively stable salinity and pH. In this regard, the study of lacustrine systems with varying salinity and pH provides a more complete picture of how nitrogen behaves in natural systems with more extreme compositions. This is critical for precise reconstructions of paleoenvironmental conditions based on $\delta^{15}\text{N}$.

From modern lakes, it is known that $\delta^{15}\text{N}$ values vary widely. Sediments from freshwater lakes display an average $\delta^{15}\text{N}$ value around 3‰, while modern alkaline lake sediments (pH > 9) fall around a mean of 13.7‰ (McLauchlan et al., 2013; Stüeken et al., 2015b), likely reflecting a much greater variety of processes than in marine environments. The $\delta^{15}\text{N}$ value of marine sediments in geological history generally does not exceed 10‰ or 12‰ as a conservative boundary (Sigman et al., 2009). Unlike the marine nitrogen cycle, ammonia volatilization from lake waters can drive the $\delta^{15}\text{N}$ value in lake sediments above the threshold of about 10–12‰ when the pH value is close to or greater than roughly 9 (Stüeken et al., 2020). Therefore, in lake environments where the pH value changes greatly, ammonia volatilization plays a significant role in the biological nitrogen cycle and its isotopic record. This phenomenon is unknown from marine settings.

To better constrain the effects of diverse environmental parameters on the nitrogen cycle, the present study is designed specifically to test how water chemistry influences nitrogen isotope ratios in the sedimentary record. We focus on multiple sets of Carboniferous to Paleogene sedimentary rocks in Chinese ancient lakes (Fig. 1), which reflect diverse sedimentary depositional environments and water chemistries, ranging in salinity from fresh to hypersaline, with compositions ranging from sodium carbonate- to sulfate-type, and displaying diverse redox states from oxic to anoxic. Our sample suite can therefore serve as a natural laboratory for systematically exploring the effects of water chemistry (i.e., salinity and pH) on nitrogen isotopes and biogeochemical cycling.

2. Samples and methods

2.1 Samples

We collected 146 lacustrine sediment samples from six basins in China (Fig. 1; Tables 1–2). Among the 66 samples of the unit $\text{C}_2\text{--P}_1\text{f}$ (the Permo–Carboniferous Fengcheng Formation) in the Junggar Basin, 56 were previously studied by Xia et al. (2020b). We include those data here for comparison. According to previous studies, the $\text{C}_2\text{--P}_1\text{f}$ sedimentary package was deposited in a strongly reducing, hypersaline, alkaline environment associated with strong volcanic–hydrothermal activity (Cao et al., 2020; Xia et al., 2020b). These conditions resulted in deposition of abundant alkaline minerals, such as wegscheiderite, trona, nahcolite, shortite, northupite, and eitelite, that provide evidence of high-pH waters (Cao et al., 2020). The Fengcheng Fm is further divided from base to top into the first (F_1), second (F_2), and third (F_3) members (Cao et al., 2005, 2020). P_2l (the middle Permian

Lucaogou Formation) is located in the Jimusar Sag in the southeastern Junggar Basin, and consists of lacustrine dolomitic–clastic rocks deposited in suboxic–anoxic and brackish–saline settings (Luo et al., 2018; Ding et al., 2020). P_{2l} also contains sporadic occurrences of shortite (a transitional Na-carbonate mineral) in the absence of typical Na-carbonate minerals such as trona, which provide evidence that the Lucaogou Formation might have been deposited during the early stages of a lake that was evolving towards an alkaline water composition (Xia et al., 2021). Regarding the other samples from the Junggar Basin, the salinity and redox depositional conditions of P_{2p} (the middle Permian Pingdiquan Formation), C (Carboniferous), P_{1j} (the lower Permian Jiamuhe Formation), and P_{2w} (the middle Permian lower-Wuerhe Formation) were mainly deposited in oxic–suboxic and freshwater–brackish lacustrine environments, and mainly comprise sandstones, siltstones, and mudstones (Cao et al., 2005).

J_{1zd} (the lower Jurassic Da’anzhai Member of the Ziliujing Formation) in the central Sichuan Basin consists mainly of silty mudstones, mudstones, and ostracoda-bearing mudstones deposited in oxic–suboxic and freshwater–brackish lacustrine settings (Xu et al., 2017; Wang et al., 2018). In contrast, E_{2s} (the Eocene Shahejie Formation) in the Bohai Bay Basin and E_{2h} (the Eocene Hetaoyuan Formation) in the Nanxiang Basin comprise mainly shales and calcareous mudstones deposited in suboxic–anoxic and brackish–saline lacustrine settings (Wei et al., 2018; Xia et al., 2019a). Similarly, E_{2q} (the Eocene Qianjiang Formation) in the Jiangnan Basin and E_{2xg} (the Eocene Xiaganchaigou Formation) in the Qaidam Basin were also both deposited in suboxic–anoxic and brackish–saline lacustrine settings (Philp and Fan, 1987; Li et al., 2018; Liu et al., 2021). E_{2q} comprises interbedded muddy dolostones and salt rocks (e.g., glauberite and gypsum) and sandstones–mudstones. E_{2xg} consists mainly of (calcareous) mudstones intercalated with lime dolostones and salt rocks (e.g., gypsum and anhydrite).

2.2 Methods

2.2.1 Total nitrogen–sulfur–organic carbon contents, and nitrogen and organic carbon isotopes

Nitrogen–sulfur–carbon contents and total N and organic C stable isotopic data were determined at the School of Earth and Environmental Sciences, University of St. Andrews, Scotland, United Kingdom. Firstly, 6 N HCl was added to the dried sample powders (< 200 mesh) at 25 °C and left overnight to remove carbonates. The resulting residues were washed three times in 18 MΩ H₂O, and then dried in an oven overnight at 60 °C. Decarbonated powders were then weighed into Sn capsules and analyzed by flash combustion in an elemental analyzer (EA Isolink) coupled to an isotope ratio mass spectrometer (Thermo Finnigan MAT253) via a Conflo IV. USGS40, USGS41, and SGR1 were used as in-house standards. The isotopic data are expressed in delta notation relative to V-PDB for δ¹³C_{org} and air for δ¹⁵N: δ (in ‰) = $(\frac{x/yR_{\text{sample}}}{x/yR_{\text{standard}}} - 1) \times 1000$, where $\frac{x/yR}{x/yR} = \frac{^{15}\text{N}/^{14}\text{N}}{^{15}\text{N}/^{14}\text{N}}$ for nitrogen and $\frac{^{13}\text{C}/^{12}\text{C}}{^{13}\text{C}/^{12}\text{C}}$ for carbon. Precision and accuracy based on replicate analyses of SGR-1 were better than ± 0.5‰ for both carbon and nitrogen isotopes. Note that the process of removing carbonates by acid and rinsing might alter the δ¹⁵N signals from bulk ones (Brodie et al.,

2011), but the effect is generally < 1‰ (Schlacher and Connolly, 2014). Thus, the comparison of $\delta^{15}\text{N}$ between different environmental conditions is valid. Further, all samples were treated in the same way, such that the preparation method is unlikely to introduce systematic bias.

2.2.2 Carbonate carbon and oxygen isotope data

Carbonate C–O stable isotopic analyses were conducted at the School of Earth Sciences and Engineering, Nanjing University, Nanjing, China. Powdered samples (< 200 mesh) were immersed in dilute H_2O_2 of 3% for 72 h to oxidize the organic carbon in the samples. Subsequently, 20 mg of the centrifuged, dried powder was reacted with 100% H_3PO_4 at 25 °C for 12 h, and a liquid N_2 trap was used to collect pure CO_2 . The resulting CO_2 was analyzed with a MAT 253 mass spectrometer to obtain $^{13}\text{C}/^{12}\text{C}$ and $^{18}\text{O}/^{16}\text{O}$ ratios. Both $\delta^{13}\text{C}_{\text{carb}}$ and $\delta^{18}\text{O}_{\text{carb}}$ are expressed in delta notation relative to V-PDB: δ (in ‰) = $(^{x/y}\text{R}_{\text{sample}}/^{x/y}\text{R}_{\text{standard}} - 1) \times 1000$, where $^{x/y}\text{R} = ^{18}\text{O}/^{16}\text{O}$ for oxygen and $^{13}\text{C}/^{12}\text{C}$ for carbon.

2.2.3 Trace elements

Trace element analyses were conducted at the School of Earth Sciences and Engineering, Nanjing University, Nanjing, China, with an Elan DRC-e ICP-MS. Firstly, 0.05 g of sample powder (< 200 mesh), 0.5 mL of concentrated HF, and 1 mL of concentrated HNO_3 were added to sealed Teflon beakers and heated at 185°C for 12 h. The samples were cooled and then evaporated to dryness. After addition of 1 mL of concentrated HNO_3 , the samples were again evaporated to dryness. Subsequently, 2 mL of dilute HNO_3 , 1 mL of 500 ng/mL Rh internal standard, and 3 mL of H_2O were added. The mixture was then sealed and heated at 140 °C for 5 h. After cooling, 0.4 mL of the solution were transferred into a 15 mL centrifuge tube, sealed, and heated at 140 °C for 5 h. This solution was then diluted to 8–10 mL with distilled and deionized water. Finally, the sample was analyzed by ICP-MS using the Rh internal standard method for drift correction.

3. Results

Based on salinity indicators (see below), our samples can be subdivided into two salinity categories: fresh-to-brackish (J_{1z} , P_{1j} , P_{2w} , P_{2p} , and C) and brackish-to-saline ($\text{C}_2\text{--P}_{1f}$, P_{2l} , E_{2h} , E_{2s} , E_{2xq} , and E_{2q}). The latter group is further divided into circum-neutral pH (E_{2h} , E_{2s} , E_{2xq} , and E_{2q}) and alkaline pH ($\text{C}_2\text{--P}_{1f}$ and P_{2l}), based on stark differences in their evaporative alkali minerals (see below).

3.1. Fresh-to-brackish circum-neutral Group 1 (J_{1z} , P_{1j} , P_{2w} , P_{2p} , and C)

The majority of samples from this group have Sr/Ba ratios below 0.8 (average = 0.5 ± 0.3 , 1SD) and B/Ga ratios below 2.5 (avg = 1.4 ± 1.1), consistent with a fresh to brackish environment (Wei and Algeo, 2019). Total nitrogen (TN) is positively correlated with total organic carbon (TOC) across this fresh-to-brackish group ($R^2 = 0.70$; Fig. 2). $\delta^{15}\text{N}$ values range from +1‰ to +9‰ with a mean of 4.1 ± 1.7 ‰, and $\delta^{15}\text{N}$ values and TOC/TN (C/N) ratios are negatively correlated ($R^2 = 0.36$; Fig. 2d). C/N ratios and $\delta^{13}\text{C}_{\text{org}}$ values are not correlated with TOC contents (Figs. 2e–2f), and $\delta^{13}\text{C}_{\text{org}}$ values range from –32‰ to –20‰

with a mean of $-24.5 \pm 2.9\%$. The Junggar Basin strata (except C₂-P_{1f} and P_{2l}, which belong to Group 3 below) have consistently higher TOC/TS (total sulfur) ratios (mostly > 5 and up to 276) compared to the J_{1z} strata (0.7 to 13). The carbonate contents of Group 1 are relatively low (7–41 wt.%; mean = 20.7 ± 6.4 wt.%). $\delta^{13}\text{C}_{\text{carb}}$ values vary between -16% and $+5\%$ (Fig. 3), while $\delta^{18}\text{O}_{\text{carb}}$ values range between -19% and -8% (Fig. 3). $\delta^{13}\text{C}_{\text{carb}}$ and $\delta^{18}\text{O}_{\text{carb}}$ values are not correlated in this group. The samples of this group have low ratio of U/Th (mean = 0.3 ± 0.2) and low Mo contents (mean = 3.2 ± 6.7 ppm).

3.2. Brackish-to-saline circum-neutral Group 2 (E_{2h}, E_{2s}, E_{2xq}, and E_{2q})

Samples from this group are characterized by Sr/Ba (avg = 2.3 ± 1.8) and B/Ga (avg = 5.1 ± 3.9) ratios that are mostly above 0.8 and 2.5, respectively, i.e., systematically higher than those in the Group 1 and consistent with the interpretation of higher salinity. Overall, TN is well correlated with TOC ($R^2 = 0.63$) in this group (Fig. 2b). $\delta^{15}\text{N}$ values range from $+4\%$ to $+10\%$ with a mean of $+7.0 \pm 1.4\%$, higher than those of Group 1, and $\delta^{15}\text{N}$ values and C/N ratios are not related (Fig. 2d). C/N ratios and $\delta^{13}\text{C}_{\text{org}}$ values are not correlated with TOC contents (Figs. 2e–2f), and $\delta^{13}\text{C}_{\text{org}}$ values range from -29% to -23% with a mean of $-25.8 \pm 1.8\%$. Samples from this group have consistently lower TOC/TS ratios (0.3–23; mean = 3.4 ± 4.4) compared to Group 1. The carbonate contents of this group are relatively high (16–71 wt.%; mean = 43.5 ± 15.4 wt.%). $\delta^{13}\text{C}_{\text{carb}}$ values vary between -7% and $+3\%$, while $\delta^{18}\text{O}_{\text{carb}}$ values range between -12% and -2% (Fig. 3), much higher than those of Group 1. $\delta^{13}\text{C}_{\text{carb}}$ and $\delta^{18}\text{O}_{\text{carb}}$ values are also not correlated in this group. The samples of this group have higher ratio of U/Th (avg = 0.5 ± 0.2) and Mo contents (avg = 9.6 ± 6.7 ppm).

3.3. Brackish-to-saline alkaline Group 3 (C₂-P_{1f} and P_{2l})

Samples from this group show Sr/Ba (mean = 1.9 ± 1.6) and B/Ga (mean = 4.5 ± 3.6) ratios that are mostly above 0.8 and 2.5, respectively, i.e., similar to those of Group 2 and also consistent with relatively higher salinity compared to Group 1 (Wei and Algeo, 2019). TN and TOC are well correlated ($R^2 = 0.51$) in this group (Fig. 2c). The most important characteristic of this group of samples is that $\delta^{15}\text{N}$ values fall all above $+10\%$ with a mean of $18.4 \pm 3.3\%$ (Fig. 2d). These rocks are thus consistently enriched in ^{15}N compared to the previous two groups. Relatively lower values mostly occur in unit P_{2l} ($+14.0 \pm 2.3\%$). There is no correlation between $\delta^{15}\text{N}$ versus C/N, TOC versus C/N, and TOC versus $\delta^{13}\text{C}_{\text{org}}$ (Figs. 2d–2f), and $\delta^{13}\text{C}_{\text{org}}$ values range from -31% to -24% with a mean of $-27.6 \pm 1.3\%$ in this group. The P_{2l} samples tend to have higher TOC/TS ratios (median = 99) compared to unit C₂-P_{1f} (median = 1.2). The carbonate contents of this group are relatively high (7–88 wt.%; mean = 33.5 ± 16.4 wt.%). $\delta^{13}\text{C}_{\text{carb}}$ values vary between -4% and $+9\%$, while $\delta^{18}\text{O}_{\text{carb}}$ values range between -15% and 4% (Fig. 3), i.e., higher than those of previous two groups. $\delta^{13}\text{C}_{\text{carb}}$ and $\delta^{18}\text{O}_{\text{carb}}$ values of C₂-P_{1f} are positively correlated in this group ($R^2 = 0.29$), which has previously been linked to strong evaporation (Xia et al., 2020b). The samples of this group have on average the highest ratio of U/Th (mean = 1.4 ± 1.1) and Mo contents (mean = 15.7 ± 15.6 ppm). Within this group, the P_{2l} tends to have slightly lower Sr/Ba and Mo contents compared to C₂-P_{1f}.

4. Discussion

4.1. Preservation of primary geochemical signals

Diagenetic alteration effects on our data first need to be considered prior to discussing their geochemical/geological implications. For most samples, TN and TOC contents are strongly correlated (Figs. 2a–2c), indicating that most nitrogen was derived from primary organic matter rather than from detrital clay minerals (Stüeken et al., 2015, 2019). An exception to this trend is unit E_{2q} in the Jiangnan Basin, where TN and TOC contents are not well correlated, which indicates that this setting experienced some nitrogen input from detrital material or alternatively organic carbon loss during anaerobic remineralization processes where nitrogen was retained (Müller, 1977; Robinson et al., 2012). For all samples, the C/N ratios are not correlated with TOC contents (Fig. 2e). Also $\delta^{13}\text{C}_{\text{org}}$ -TOC and $\delta^{15}\text{N}$ -C/N show no correlations across the whole dataset, likely reflecting minimal or negligible thermal alteration of these samples, if any, on $\delta^{13}\text{C}_{\text{org}}$ and $\delta^{15}\text{N}$ values (Fig. 2d; Fig. 2f; Stüeken et al., 2019). Significant metamorphic alteration is only expected at greenschist facies and above (Thomazo and Papineau, 2013), which is not applicable to these rocks. Thus, the TN, $\delta^{15}\text{N}$, and $\delta^{13}\text{C}_{\text{org}}$ data likely reflect primary and early diagenetic signatures that were controlled by the environmental conditions (water chemistry) at the time of deposition, and the overall effect of early diagenesis on the $\delta^{15}\text{N}$ and $\delta^{13}\text{C}_{\text{org}}$ signals of residual biomass is minor and does not impact the data interpretations (Lehmann et al., 2002; Quan et al., 2013). This supports the validity of the subsequent discussion.

The $\delta^{13}\text{C}_{\text{carb}}$ and $\delta^{18}\text{O}_{\text{carb}}$ values show no evidence of either diagenetic alteration or petrological control, based on the absence of correlations between $\delta^{13}\text{C}_{\text{carb}}$, $\delta^{18}\text{O}_{\text{carb}}$, and carbonate contents (except some E_{2q} samples, Jiangnan Basin), and Mn/Sr ratios of <10 (Fig. 3; Kaufman and Knoll, 1995; Stüeken et al., 2019). For the exceptional E_{2q} samples, $\delta^{13}\text{C}_{\text{carb}}$ and carbonate contents have a strong negative correlation, possibly resulting from extensive diagenetic oxidation of organic matter that led to the formation of significant amounts of diagenetic carbonates (Kaufman and Knoll, 1995). Hence the negative $\delta^{13}\text{C}$ values of organic matter were inherited by the late-formed diagenetic carbonates in E_{2q}, but this process does not appear to have been significant in any of the other units. This supports the validity of the subsequent discussion.

4.2. Validity of determining paleobasicity based on $\delta^{15}\text{N}$ values

Nitrogen isotopes have been suggested as a potential proxy for basicity of ancient water mass, where $\delta^{15}\text{N} > 10\text{--}12\text{‰}$ is indicative of high-pH conditions (Deng et al., 2018; Stüeken et al., 2020). This is because above a pH value of 9.25, more than 50% of dissolved NH_4^+ decomposes to H^+ and NH_3 . Because the isotopic effects associated with NH_4^+ decomposition (Li et al., 2021) and followed NH_3 devolatilization (Deng et al., 2018) can lead to a net ^{15}N enrichment in the residual NH_4^+ for as large as 45‰ (Li et al., 2012), the process will result in an isotope enrichment of the lake residual nitrogen. Measuring such highly enriched $\delta^{15}\text{N}$ values in the sedimentary rock record could therefore be a useful tool for tracking high pH conditions in paleoenvironments (Kempe et al., 1991; Stüeken et al., 2020).

However, the validity of this proxy has so far not been well explored: in addition to 'first-order' controls by local pH conditions as outlined above, high $\delta^{15}\text{N}$ values of sediments can theoretically also result from a number of 'second-order' factors such as salinity and redox state (Collister and Hays, 1973; Quan et al., 2013; Naafs et al., 2019; Yang et al., 2019). This complexity limits our ability to apply nitrogen isotopes as a basicity proxy in deep time.

The $\delta^{15}\text{N}$ values of the environmentally and chemically diverse localities analyzed in this study vary markedly (1.2‰–24.4‰; Fig. 4), which likely indicates a great variety of processes. The threshold of +10–12‰ for alkaline water bodies (Stüeken et al., 2020) is supported by the observation that higher values (>10–12‰) almost exclusively occur in C₂–P_{1f} and P_{2l} in the Junggar Basin, where alkali minerals and organic biomarkers provide independent evidence for high pH (Cao et al., 2020; Xia et al., 2021). Extensive previous work on the C₂–P_{1f} unit revealed a complete sedimentary evolution sequence of an archetypal alkaline lake, including evidence for the presence of alkali minerals such as trona and shortite, globular bacteria-like fossils, low contents of clay minerals, inorganic geochemistry indicating high salinity, strongly reducing conditions, and hydrothermal activity (Cao et al., 2020). Lipid biomarkers of C₂–P_{1f} also indicate the saline and redox-stratified lacustrine condition, similar to typical modern and ancient saline alkaline lakes (Cao et al., 2020; Xia et al., 2020a). These signatures included moderately high gammacerane/C₃₀ $\alpha\beta$ hopane ratios, no detectable signal of 24-n-propylcholestanes from marine pelagophyte algae, high amounts of preserved β -carotane, and low pristane/phytane ratios (Cao et al., 2020; Xia et al., 2020a). Unit P_{2l}, which also shows elevated $\delta^{15}\text{N}$ values, contains sporadic occurrences of shortite (a transitional Na-carbonate mineral) in the absence of typical Na-carbonate minerals such as trona, which provide strong evidence that the P_{2l} might have been deposited during the early stages of an alkaline lake (Xia et al., 2021).

In contrast to all the samples from alkaline Group 3, the $\delta^{15}\text{N}$ values of the circum-neutral ancient lakes (Group 1 and Group 2) in this study, which lack independent mineralogical evidence of high pH, have $\delta^{15}\text{N}$ values <10–12‰ (Fig. 4). This argues for the validity of the threshold of +10–12‰ to distinguish alkaline and circum-neutral water mass. This is further supported by the nitrogen isotopic composition of modern Lake Bosumtwi, Ghana, where the $\delta^{15}\text{N}$ values greater than 12‰ occur in sediments in the interval of 13.5–20 kyr B.P., concurrent with high pH and reflecting NH_3 volatilization (Talbot and Johannessen, 1992). In contrast, roughly >90% of modern ocean core tops (related to either denitrification or uptake fractionation processes rather than pH) have $\delta^{15}\text{N}$ values lower than 10‰ (Tesdal et al., 2013). Overall, these data are therefore consistent with the proposition that $\delta^{15}\text{N}$ can serve as a basicity proxy, because in our sample set it successfully replicates the mineralogical contrast between Group 3 on the one hand and Groups 1 and 2 on the other hand. We recommend a threshold of 10–12‰ rather than an absolute value because the pH condition that may induce significant NH_3 degassing also varies depending on temperature and mass balance of the $\text{NH}_4^+/\text{NH}_3$ pool between supply and consumption (Li et al., 2012).

4.3. Influence of salinity on $\delta^{15}\text{N}$ values

Multiple salinity proxies were used in the present study (Degens et al., 1957; Berner and

Raiswell, 1984; Horton et al., 2016; Wei and Algeo, 2019), including $\delta^{18}\text{O}_{\text{carb}}$, TOC/TS, Sr/Ba and B/Ga to distinguish between fresh and saline water masses (Fig. 5). $\delta^{18}\text{O}_{\text{carb}}$ values increase with salinity because isotopically light H_2O and CO_2 are preferentially lost during evaporation (Horton et al., 2016). However, $\delta^{18}\text{O}_{\text{carb}}$ values cannot be used to reconstruct differences in salinities between different lakes, as the lakes were formed at different times in Earth's history and in different locations and thus it is very unlikely that the starting composition of rain water was the same. $\delta^{18}\text{O}_{\text{carb}}$ is therefore only used as a salinity proxy within individual lake basins such as C₂–P_{1f} in the Junggar Basin with a given geological setting. We take the $\delta^{18}\text{O}_{\text{carb}}$ as the salinity proxy in alkaline Group 3 because the other proxies (TOC/TS, Sr/Ba and B/Ga ratios) were likely affected by hydrothermal alteration in this particular basin and $\delta^{18}\text{O}_{\text{carb}}$ best records the true water salinity of the alkaline C₂–P_{1f} strata (Xia et al., 2020b). The $\delta^{18}\text{O}_{\text{carb}}$ of C₂–P_{1f} in the Junggar Basin was most likely not severely affected by hydrothermal alteration as a majority of $\delta^{18}\text{O}_{\text{carb}}$ is greater than -10% (Fig. 3a). The variation of salinity is supported by the co-variation of abundance of evaporite minerals precipitating from the saline water. The TOC/TS, Sr/Ba and B/Ga proxies are applicable for other groups in this study (Fig. 5) (Wei and Algeo, 2019).

Based on these proxies, we categorized all samples in this study into fresh-to-brackish circum-neutral Group 1 (J_{1zd} and other formations in the Junggar Basin), brackish-to-saline circum-neutral Group 2 (E_{2h}, E_{2s}, E_{2xq}, and E_{2q}), and brackish-to-saline alkaline Group 3 (C₂–P_{1f} and P_{2l}) (Fig. 5). It should be noted that the environmental conditions in each stratum are certainly variable, but the salinity variability within groups is smaller than the systematic differences between groups. Furthermore, given the wide range of salinities indicated by different proxies, it is possible that the data were variably affected by diagenesis and/or differences in mineralogy during deposition. These effects are minimized by using multiple proxies together and by combining samples from the same geological formation that share a similar provenance and diagenetic history. For example, E_{2q} would be grouped as mostly saline according to Sr/Ba, midrange based on TOC/TS, and less saline using B/Ga (Fig. 5); however, despite this variability, the important point is that no samples of E_{2q} belong to the fresh water category based on Sr/Ba and only one sample would be classified as fresh water based on TOC/TS and B/Ga, so E_{2q} overall can be placed into the brackish-to-saline circum-neutral Group 2. It is entirely possible that environmental conditions changed within the given interval, because rapid temporal variability is one of the intrinsic properties of lakes. However, this study is focused on long-term, first-order differences in salinity. Grouping samples into larger salinity categories is therefore a valid approach. The strategy of using a fine sampling density that can resolve seasonal or annual fluctuations could be conducted in the future to investigate higher-order linkages between salinity and nitrogen cycling that are not the focus of this study.

To assess the first-order impact of salinity, we examined correlations between salinity proxies and $\delta^{15}\text{N}$ values across all lakes (Fig. 4). Within Groups 1, 2, and 3, respectively, we do not observe a direct correlation or only weak correlation between salinity proxies and $\delta^{15}\text{N}$ (Fig. 4). These weak correlations indicate that salinity does not exert a direct control on $\delta^{15}\text{N}$; however, it may have secondary effects as discussed below.

For Groups 1 and 2, both groups are inferred to have been circum-neutral (i.e., non-alkaline, Section 3). However, Group 2, which represents a more saline sedimentary environment (mean Sr/Ba = 2.3 ± 1.8 , mean B/Ga ratios = 5.1 ± 3.9 , and mean TOC/TS = 3.4 ± 4.3) than Group 1, has systematically higher $\delta^{15}\text{N}$ values (mean = $7.0 \pm 1.4\text{‰}$) than those of the less saline Group 1 (mean $\delta^{15}\text{N}$ = $4.1 \pm 1.7\text{‰}$, mean Sr/Ba = 0.5 ± 0.3 , mean B/Ga ratios = 1.4 ± 1.1 , and mean TOC/TS = 40.4 ± 65.0). Hence, even though there is no direct correlation on a sample-by-sample basis, this broad first-order covariance between salinity and $\delta^{15}\text{N}$ in circum-neutral groups suggests that different processes are occurring at elevated salinity, affecting nitrogen isotope fractionation.

One of the possible explanations to this co-variation between salinity and $\delta^{15}\text{N}$ in circum-neutral groups is an increase of water column denitrification under more saline conditions. For the circum-neutral groups, where ammonia volatilization is insignificant, $\delta^{15}\text{N}$ values were probably mainly controlled by redox processes (Talbot, 2001; Quan et al., 2013), in particular denitrification, which preferentially removes ^{14}N from the water column (as shown in Fig. 6 in detail where circum-neutral groups are mainly controlled by denitrification rather than NH_3 volatilization as in the alkaline group). We speculate that elevated salinity leads to an increase in the ratio of water-column to sedimentary denitrification (Quan et al., 2013). Denitrification in the water column imparts an average isotopic effect of -25‰ , while in sediments the net isotopic effect is close to 0‰ (Kessler et al., 2014). If an increase in water salinity intensifies the stratification of the water body, leading to stagnation and deoxygenation of lake bottom waters, relatively more denitrification occurs in the water column, such that more isotopically light N_2 is released into the atmosphere and the remaining NO_3^- becomes more ^{15}N -enriched. Therefore, our observations suggest that in general more saline environments have a tendency to preserve higher $\delta^{15}\text{N}$ values, possibly due to redox processes as described above. However, we stress the absence of a direct correlation between salinity and sedimentary $\delta^{15}\text{N}$, because the linkage is complex and likely affected by other variables such as temperature, depth of the chemocline, and productivity.

Another possible explanation for the co-variation between salinity and $\delta^{15}\text{N}$ value in the circum-neutral groups is the source of the organic matter and/or ecological shifts. In the less saline Group 1, the lowest values in $\delta^{15}\text{N}$ tend to occur in samples with high C/N ratios ($R^2 = 0.36$; Fig. 7a). As terrestrial plant biomass is characterized by high C/N ratios (>30 ; Reich and Oleksyn, 2004) and a mode in global average $\delta^{15}\text{N}$ close to 0‰ (Craine et al., 2009), the inputs of terrestrial plants could potentially contribute to the high C/N ratios (mostly higher than 20) and low $\delta^{15}\text{N}$ values (mostly lower than 5‰) in Group 1, which is consistent with fossils of higher plants in Group 1 (Qin et al., 2021). Input of fern plants would perhaps also explain the relatively high $\delta^{13}\text{C}_{\text{org}}$ values (up to -20‰) in some samples of Group 1, if this terrestrial biomass had a distinct carbon isotopic composition relative to simple aquatic algae. This is unknown, but possible. The lowest $\delta^{15}\text{N}$ values tend to be in samples with high C/N ratios and enriched $\delta^{13}\text{C}_{\text{org}}$ values ($R^2 = 0.36$; Fig. 7b), which indicates that the high inputs from terrestrial plants in fresh-to-brackish lake water may result in low $\delta^{15}\text{N}$ values in Group 1. In the more saline Group 2, there is no trend between $\delta^{15}\text{N}$ and C/N ratio ($R^2 = 0.02$; Fig. 7c) or between $\delta^{15}\text{N}$ and $\delta^{13}\text{C}_{\text{org}}$ ($R^2 = 0.07$; Fig. 7d); C/N ratios and $\delta^{13}\text{C}_{\text{org}}$ values are mostly

below 20 and -24% , respectively. This pattern might indicate that these saline lakes were inhabited by more algal and bacterial biomass as opposed to higher plants (Cloern et al., 2002). This model would explain why $\delta^{15}\text{N}$ does not drop as much with increasing C/N ratios (resulting from diagenesis) and $\delta^{13}\text{C}_{\text{org}}$ values (reflecting variable metabolic pathways). Therefore, with increasing salinity from Group 1 to Group 2, the shift from terrestrial plants to aquatic algae and bacteria as main primary producers, paired with increasing stratification and water-column denitrification, may account for the increasing $\delta^{15}\text{N}$ values.

We emphasize that a decrease in terrestrial plant biomass to the lake sediments under relatively more saline conditions could be caused by either a direct decline in higher aquatic plants that were producing organic matter in-situ (i.e., autochthonous), or it could reflect a generally hotter and drier climate in the region around the lake that caused a decline in the amount of plant debris from the surroundings (i.e., allochthonous) (Talbot and Johannessen, 1992; Cloern et al., 2002). It is also possible that both factors contributed, which would further explain why we see no direct strong correlation between salinity and $\delta^{15}\text{N}$. However, our first-order observation remains that saline environments tend to favor elevated $\delta^{15}\text{N}$ values – either through associated redox processes within the water column, or through associated changes in the local biota, or other processes not discussed here.

4.4. Relationship between $\delta^{15}\text{N}$ and redox state

To further explore the effects of redox conditions noted above in the context of salinity, we investigated U/Th ratios and Mo abundances as redox proxies (Jones and Manning, 1994; Scott and Lyons, 2012). In our data set, U/Th ratios show very little variation (with the exception of the C₂-P_{1f} samples, which have experienced hydrothermal input; Fig. 8a; Xia et al., 2020b). The C₂-P_{1f} hydrothermal activity in this study is parasynthetic (a bit eogenetic at most) based on the fact that the studied Mahu Sag experienced extensional tectonic settings with intense volcanic activity during the time of sediment deposition (Carroll et al., 1995; Wartes et al., 2002). Those factors likely drove hydrothermal activity while the basin was active. Therefore, the rock data are influenced by hydrothermal input to the ancient lake water column, and the U/Th proxy is not exclusively driven by redox changes in the C₂-P_{1f} samples. However, Mo does show a wider range across all samples, independently from hydrothermal input to the C₂-P_{1f} samples, and will therefore be applied to assess at least relative differences in redox (Fig. 8a). In general, molybdenum becomes progressively more enriched in sediments with increasing anoxia (Jones and Manning, 1994; Scott and Lyons, 2012) (Fig. 8). There are caveats to using Mo abundances or other redox proxies in lakes, because high sedimentation rates can dilute Mo concentrations and saline waters may be more Mo-rich independent of the redox state. Another caveat is the condition of the lacustrine basins as some basins are endorheic and others are exorheic, and they receive input from different source rocks (Tapia et al., 2018). This complexity highlights the difficulty of reconstructing paleo-redox conditions from lacustrine basins where no reliable proxy has been developed to date (Bennett and Canfield, 2020).

Nevertheless, large Mo enrichments of several ppm (relative to 1–2 ppm in average crust, Hans Wedepohl, 1995) cannot easily be explained without a redox control. In saline lakes, the

contents of dissolved O₂ in the water column commonly decrease with increasing salinity, because O₂ gas becomes less soluble (Fig. 8b; Warren, 2016). TOC/TS ratios in our sample set have a moderate negative correlation with Mo content (Fig. 8c), suggesting that more saline lake waters (lower TOC/TS) may be associated with increasingly reducing conditions that favored Mo drawdown into sediments (Warren, 2016). We note that Sr/Ba and B/Ga ratios are not well correlated with Mo content (Fig. 8d). It is possible that Sr/Ba and B/Ga are not sufficiently reliable salinity proxies, or more likely, that these lakes did not accumulate significant amounts of Mo in the water column, despite high concentrations of other salts (Algeo and Tribovillard, 2009; Wei and Algeo, 2019). However, given the first-order trend of high Mo abundances in many of the more saline samples, we conclude that changes in $\delta^{15}\text{N}$ with increasing salinity are most likely related to expansion of anoxic conditions due to stagnation of the water column and decreasing O₂ solubility (Fig. 8b).

As discussed above, for circum-neutral Group 1 and Group 2, our first explanation was that suboxic to anoxic bottom waters resulting from salinity stratification may have led to water column denitrification and increasing $\delta^{15}\text{N}$ values in residual nitrate and nitrate-assimilating biomass. Under strongly anoxic conditions, $\delta^{15}\text{N}$ would be expected to return to lower values, because nitrate is reduced so rapidly in strongly anoxic conditions that the residual nitrate would not leave a significant trace in the sediment record (Fig. 9; Quan et al., 2013). Under fully oxic conditions, denitrification only occurs in sediments, such that $\delta^{15}\text{N}$ values are close to the originally fixed nitrogen with a small isotopic fractionation (Fig. 9; Quan et al., 2013). In our case, we do indeed observe relatively low Mo abundances near crustal background levels in the non-saline samples of Group 1, which also show relatively lower $\delta^{15}\text{N}$ values (Fig. 9). In contrast, the more saline samples from Group 2 tend to be Mo-enriched. This trend supports our interpretation that salinity is linked to redox shifts in the water column. The combination of higher salinity and anoxia may therefore have increased $\delta^{15}\text{N}$ values in the circum-neutral lakes.

Under alkaline conditions, $\delta^{15}\text{N}$ values would be expected to increase with increasingly reducing lake water due to enhanced NH₃ volatilization. NH₃ is more likely to escape into the atmosphere from reducing waters, because under oxic conditions it would be readily oxidized and remain in the water column, as observed in modern alkaline lakes where NH₃ escapes during seasonal overturn of the stratified water column (Jellison et al., 1993; Stüeken et al., 2015b). We do not observe a direct correlation between Mo abundances and $\delta^{15}\text{N}$ ($R^2 = 0.2$), which underpins the redox state is not the primary controlling factor of the $\delta^{15}\text{N}$ value in alkaline lakes. Although NH₃ degassing requires anoxia, it is not necessarily correlated with redox. As long as conditions are sufficiently anoxic to accumulate an NH₃ reservoir somewhere in the water column from where it can (seasonally) degas, a further decrease in redox potential would not necessarily change the degree of NH₃ degassing. Hence a sample-by-sample covariance between Mo abundances and $\delta^{15}\text{N}$ is not expected. Our samples from Group 3 are generally enriched in Mo compared to average crust (Figs. 8–9), reflecting anoxic conditions, which would have promoted NH₃ escape. As our samples of Group 3 were mostly deposited in suboxic to anoxic conditions (Cao et al., 2020; Xia et al., 2020a), the possibility that nitrate was the main form of nitrogen and therefore prohibited

NH₃ volatilization can be ruled out. Hence similar to salinity in the circum-neutral lakes (Groups 1 and 2), where redox was the most important controlling factor for nitrogen isotopes, redox conditions in alkaline lakes, where NH₃ volatilization dominates, only have secondary influence on $\delta^{15}\text{N}$ values. In other words, we can identify a hierarchy of effects on nitrogen isotopes:

- pH > 9 and anoxic (+/- saline): NH₃ volatilization dominates, $\delta^{15}\text{N} > 10\text{--}12\text{‰}$
- pH < 9 and anoxic (+/- saline): water-column redox reactions dominate, where anoxia is promoted by high salinity, $\delta^{15}\text{N} < 10\text{--}12\text{‰}$
- pH > or < 9 and oxic: primary biomass and diagenetic processes dominate, $\delta^{15}\text{N} \sim 0\text{--}5\text{‰}$

4.5. Implications

Overall, our comparison of paleo-lakes in China with vastly different properties revealed several important insights into the linkages between nitrogen cycling, nitrogen isotopic ratios and other environmental properties. We provide a more complete picture of how nitrogen behaves in natural systems with more extreme compositions compared with studies in marine sediments. Our results are consistent with the proposition that the threshold of 10–12‰ works to distinguish alkaline and circum-neutral water masses in general according to our Phanerozoic samples.

For the lakes with circum-neutral condition in this study, the biological nitrogen cycle is mainly controlled by redox processes and biomass source. $\delta^{15}\text{N}$ values are usually lower than 10–12‰. Salinity imparts an overall control on shifts in redox conditions and ecology, but other factors, such as the water source, water temperature, depth of the chemocline, and primary productivity, which were not investigated here might also affect $\delta^{15}\text{N}$ signals (Gu, 2009; Stüeken et al., 2016).

Sample-by-sample correlations between salinity, redox, and $\delta^{15}\text{N}$ were not observed in this study, which implies an "on-off" effect. For example, in the alkaline lake, NH₃ is produced in large quantities when the redox potential is sufficiently low and pH is higher than 9, but once this threshold is reached, a further reduction of the redox potential or increase in pH may not necessarily translate into an additional isotopic shift in $\delta^{15}\text{N}$. Similarly, increasing salinity may lead to stagnation and anoxia conducive to denitrification in the water column, but once all nitrate is removed, a further decrease in redox potential cannot enhance denitrification any further and therefore one would not expect a gradual change in $\delta^{15}\text{N}$ in covariance with salinity.

To sum up, our results thus show that the marine biological nitrogen cycle does not reveal the full extent of biogeochemical processes that affect nitrogen isotopic ratios in sedimentary archives. Other parameters, in particular pH and salinity, need to be considered when applying this proxy to ancient rocks on Earth and beyond Earth.

5. Conclusions

The lacustrine sediments that we investigated fall into three groups based on salinity proxies and evaporative alkali minerals: fresh-to-brackish circum-neutral Group 1,

brackish-to-saline circum-neutral Group 2, and brackish-to-saline alkaline Group 3. Circum-neutral Group 1 (average $\delta^{15}\text{N} = 4.1 \pm 1.7\text{‰}$) and Group 2 (average $\delta^{15}\text{N} = 7.0 \pm 1.4\text{‰}$) are characterized with $\delta^{15}\text{N} < +10\text{--}12\text{‰}$ while alkaline Group 3 (average $\delta^{15}\text{N} = 18.4 \pm 3.3 \text{‰}$) with $\delta^{15}\text{N} > +10\text{--}12\text{‰}$.

The $\delta^{15}\text{N}$ values are not directly correlated with lake salinity and redox state with low R^2 , but they show a broad covariance with these parameters, indicating that redox and salinity affect processes within the nitrogen cycle. $\delta^{15}\text{N}$ values of the Group 1 and Group 2 were likely controlled by denitrification, and those of the alkaline Group 3 were mainly controlled by NH_3 volatilization. The co-variation of $\delta^{15}\text{N}$ values and salinity may also be caused by the change of biological composition indicated by variation of C/N ratios and $\delta^{13}\text{C}_{\text{org}}$ values. A return to lower $\delta^{15}\text{N}$ values in Group 1 and Group 2 under strongly anoxic conditions may be indicated in our data and would be expected for a nitrogen cycle that becomes entirely anaerobic.

$\delta^{15}\text{N}$ variation in lacustrine environments is significantly greater than that in marine environments, indicative of sharply different nitrogen geochemistry and cycling during sediment deposition and subsequent diagenesis. Although we were unable to monitor other parameters such as lake size, temperature, productivity, or sedimentation rates, our results show that in lakes, salinity-induced redox stratification and basicity-induced ammonia degassing have strong first-order effects on nitrogen biogeochemical cycling.

Acknowledgments

We thank editors Brad Singer and Ganqing Jiang, and reviewers Magali Ader and Long Li for their insightful comments in improving the manuscript. This work was funded by the National Natural Science Foundation of China (Grant No. 41830425). EES acknowledges funding from a NERC grant (NE/V010824/1).

References

- Algeo, T.J., and Tribovillard, N., 2009, Environmental analysis of paleoceanographic systems based on molybdenum-uranium covariation: *Chemical Geology*, v. 268, p. 211–225, doi:10.1016/j.chemgeo.2009.09.001.
- Bennett, W.W., and Canfield, D.E., 2020, Redox-sensitive trace metals as paleoredox proxies: A review and analysis of data from modern sediments: *Earth-Science Reviews*, v. 204, p. 103175, doi:10.1016/j.earscirev.2020.103175.
- Berner, R.A., and Raiswell, R., 1984, Geology C / S method for distinguishing freshwater from marine sedimentary rocks Geological Society of America C / S method for distinguishing freshwater from marine sedimentary rocks: *Geology*, v. 12, p. 365–368, doi:10.1130/0091-7613(1984)12<365.
- Brodie, C.R., Leng, M.J., Casford, J.S.L., Kendrick, C.P., Lloyd, J.M., Yongqiang, Z., and Bird, M.I., 2011, Evidence for bias in C and N concentrations and $\delta^{13}\text{C}$ composition of terrestrial and aquatic organic materials due to pre-analysis acid preparation methods: *Chemical Geology*, v. 282, p. 67–83, doi:10.1016/j.chemgeo.2011.01.007.
- Brunner, B. et al., 2013, Nitrogen isotope effects induced by anammox bacteria: *Proceedings*

- of the National Academy of Sciences of the United States of America, v. 110, p. 18994–18999, doi:10.1073/pnas.1310488110.
- Cao, J., Xia, L., Wang, T., Zhi, D., Tang, Y., and Li, W., 2020, An alkaline lake in the Late Paleozoic Ice Age (LPIA): A review and new insights into paleoenvironment and petroleum geology: *Earth-Science Reviews*, v. 202, p. 1–14, doi:10.1016/j.earscirev.2020.103091.
- Cao, J., Zhang, Y., Hu, W., Yao, S., Wang, X., Zhang, Y., and Tang, Y., 2005, The Permian hybrid petroleum system in the northwest margin of the Junggar Basin, northwest China: *Marine and Petroleum Geology*, v. 22, p. 331–349, doi:10.1016/j.marpetgeo.2005.01.005.
- Carroll, A.R., Graham, S.A., Hendrix, M.S., Ying, D., and Zhou, D., 1995, Late Paleozoic tectonic amalgamation of northwestern China: sedimentary record of the northern Tarim, northwestern Turpan, and southern Junggar Basins: *Geological Society of America Bulletin*, v. 107, p. 571–594, doi:10.1130/0016-7606(1995)107<0571:LPTAON>2.3.CO;2.
- Casciotti, K.L., 2009, Inverse kinetic isotope fractionation during bacterial nitrite oxidation: *Geochimica et Cosmochimica Acta*, v. 73, p. 2061–2076, doi:10.1016/j.gca.2008.12.022.
- Cloern, J.E., Canuel, E.A., and Harris, D., 2002, Stable carbon and nitrogen isotope composition of aquatic and terrestrial plants of the San Francisco Bay estuarine system: *Limnology and Oceanography*, v. 47, p. 713–729, doi:10.4319/lo.2002.47.3.0713.
- Collister, J.W., Hays, J. M., 1973, A preliminary study of carbon and nitrogen isotopic biogeochemistry of lacustrine sedimentary rocks from the Green River Formation, Wyoming, Utah, and Colorado. In: Tuttle M.L. (Ed.), *Geochemical, Biogeochemical, and Sedimentological Studies of the Green River Formation, Wyoming, Utah, and Colorado*. U.S. Geological Survey, Denver, CO, pp. 265–276
- Craine, J.M. et al., 2009, Global patterns of foliar nitrogen isotopes and their relationships with climate, mycorrhizal fungi, foliar nutrient concentrations, and nitrogen availability: *New Phytologist*, v. 183, p. 980–992, doi:10.1111/j.1469-8137.2009.02917.x.
- Degens, E.G., Williams, M.L., and Keith, M. L., 1957, Environmental studies of Carboniferous sediments. Part I: geochemical criteria for differentiating marine from fresh-water shales: *AAPG Bulletin*, v. 41, p. 2427–2455, doi:10.1306/0BDA59A5-16BD-11D7-8645000102C1865D.
- Deng, Y., Li, Y., and Li, L., 2018, Experimental investigation of nitrogen isotopic effects associated with ammonia degassing at 0–70 °C: *Geochimica et Cosmochimica Acta*, v. 226, p. 182–191, doi:10.1016/j.gca.2018.02.007.
- Ding, W., Hou, D., Jiang, L., Jiang, Y., and Wu, P., 2020, High abundance of carotenes in the brackish-saline lacustrine sediments : A possible cyanobacteria source ? *International Journal of Coal Geology*, v. 219, p. 103373, doi:10.1016/j.coal.2019.103373.
- Godfrey, L. V., and Glass, J.B., 2011, The geochemical record of the ancient nitrogen cycle, nitrogen isotopes, and metal cofactors, *in Methods in Enzymology*, Academic Press Inc., v. 486, p. 483–506, doi:10.1016/B978-0-12-381294-0.00022-5.

- Gu, B., 2009, Variations and controls of nitrogen stable isotopes in particulate organic matter of lakes: *Oecologia*, v. 160, p. 421–431, doi:10.1007/s00442-009-1323-z.
- Hans Wedepohl, K., 1995, The composition of the continental crust: *Geochimica et Cosmochimica Acta*, v. 59, p. 1217–1232, doi:10.1016/0016-7037(95)00038-2.
- Horton, T.W., Defliese, W.F., Tripathi, A.K., and Oze, C., 2016, Evaporation induced ^{18}O and ^{13}C enrichment in lake systems: A global perspective on hydrologic balance effects: *Quaternary Science Reviews*, v. 131, p. 365–379, doi:10.1016/j.quascirev.2015.06.030.
- Javor, B.J., 1983, Planktonic standing crop and nutrients in a saltern ecosystem: *Limnology and Oceanography*, v. 28, p. 153–159, doi:10.4319/lo.1983.28.1.0153.
- Javor, B.J., 1985, Nutrients and ecology of the Western Salt, Exportadora de Sal saltern brines. In: Schreiber, B.C. (Ed.), *Sixth Symposium on Salt*, vol. 1, The Salt Institute, Alexandria, pp. 195–205.
- Jellison, R., Miller, L.G., Melack, J.M., and Dana, G.L., 1993, Meromixis in hypersaline Mono Lake, California. 2. Nitrogen fluxes: *Limnology and Oceanography*, v. 38, p. 1020–1039, doi:10.4319/lo.1993.38.5.1020.
- Jones, B., and Manning, D.A.C., 1994, Comparison of geochemical indices used for the interpretation of palaeoredox conditions in ancient mudstones: *Chemical Geology*, v. 111, p. 111–129, doi:10.1016/0009-2541(94)90085-X.
- Kaufman, A.J., and Knoll, A.H., 1995, Neoproterozoic variations in the C-isotopic composition of seawater: stratigraphic and biogeochemical implications: *Precambrian Research*, v. 73, p. 27–49, doi:10.1016/0301-9268(94)00070-8.
- Kempe, S., Kazmierczak, J., Landmann, G., Konuk, T., Reimer, A., and Lipp, A., 1991, Largest Known microbialites discovered in Lake Van, Turkey: *Nature*, v. 349, p. 605–608, doi:10.1038/349605a0.
- Kessler, A.J., Bristow, L.A., Cardenas, M.B., Glud, R.N., Thamdrup, B., and Cook, P.L.M., 2014, The isotope effect of denitrification in permeable sediments: *Geochimica et Cosmochimica Acta*, v. 133, p. 156–167, doi:10.1016/j.gca.2014.02.029.
- Lehmann, M.F., Bernasconi, S.M., Barbieri, A., and McKenzie, J.A., 2002, Preservation of organic matter and alteration of its carbon and nitrogen isotope composition during simulated and in situ early sedimentary diagenesis: *Geochimica et Cosmochimica Acta*, v. 66, p. 3573–3584, doi:10.1016/S0016-7037(02)00968-7.
- Li, M., Chen, Z., Cao, T., Ma, X., Liu, X., Li, Z., Jiang, Q., and Wu, S., 2018, Expelled oils and their impacts on Rock-Eval data interpretation, Eocene Qianjiang Formation in Jiangnan Basin, China: *International Journal of Coal Geology*, v. 191, p. 37–48, doi:10.1016/j.coal.2018.03.001.
- Li, L., He, Y., Zhang, Z., and Liu, Y., 2021, Nitrogen isotope fractionations among gaseous and aqueous NH_4^+ , NH_3 , N_2 , and metal-ammine complexes: Theoretical calculations and applications: *Geochimica et Cosmochimica Acta*, v. 295, p. 80–97, doi:10.1016/j.gca.2020.12.010.
- Li, L., Lollar, B.S., Li, H., Wortmann, U.G., and Lacrampe-Couloume, G., 2012, Ammonium stability and nitrogen isotope fractionations for NH_4^+ - $\text{NH}_3(\text{aq})$ - $\text{NH}_3(\text{gas})$ systems at 20-70°C and pH of 2-13: Applications to habitability and nitrogen cycling in

- low-temperature hydrothermal systems: *Geochimica et Cosmochimica Acta*, v. 84, p. 280–296, doi:10.1016/j.gca.2012.01.040.
- Liu, C., Liu, K., Wang, X., Wu, L., and Fan, Y., 2019, Chemostratigraphy and sedimentary facies analysis of the Permian Lucaogou Formation in the Jimusaer Sag, Junggar Basin, NW China: Implications for tight oil exploration: *Journal of Asian Earth Sciences*, v. 178, p. 96–111, doi:10.1016/j.jseaes.2018.04.013.
- Liu, Z., Zhang, Y., Song, G., Li, S., Long, G., Zhao, J., Zhu, C., Wang, Y., Gong, Q., and Xia, Z., 2021, Mixed carbonate rocks lithofacies features and reservoirs controlling mechanisms in a saline lacustrine basin in Yingxi area, Qaidam Basin, NW China: *Petroleum Exploration and Development*, v. 48, p. 80–94, doi:10.1016/S1876-3804(21)60006-X.
- Luo, Q., Gong, L., Qu, Y., Zhang, K., Zhang, G., and Wang, S., 2018, The tight oil potential of the Lucaogou Formation from the southern Junggar Basin, China: *Fuel*, v. 234, p. 858–871, doi:10.1016/j.fuel.2018.07.002.
- McLauchlan, K.K., Williams, J.J., Craine, J.M., and Jeffers, E.S., 2013, Changes in global nitrogen cycling during the Holocene epoch: *Nature*, v. 495, p. 352–355, doi:10.1038/nature11916.
- Mitchell, B.D., and Geddes, M.C., 1977, Distribution of the brine shrimps *Parartemia zietziana* Sayce and *Artemia salina* (L.) along a salinity and oxygen gradient in a South Australian saltfield: *Freshwater Biology*, v. 7, p. 461–467, doi:10.1111/j.1365-2427.1977.tb01695.x.
- Müller, P.J., 1977, C N ratios in Pacific deep-sea sediments: Effect of inorganic ammonium and organic nitrogen compounds sorbed by clays: *Geochimica et Cosmochimica Acta*, v. 41, p. 765–776, doi:10.1016/0016-7037(77)90047-3.
- Naafs, B.D.A., Monteiro, F.M., Pearson, A., Higgins, M.B., Pancost, R.D., and Ridgwell, A., 2019, Fundamentally different global marine nitrogen cycling in response to severe ocean deoxygenation: *Proceedings of the National Academy of Sciences of the United States of America*, v. 116, p. 24979–24984, doi:10.1073/pnas.1905553116.
- Philp, R.P., and Fan, Z.A., 1987, Geochemical investigation of oils and source rocks from Qianjiang depression of Jiangnan basin, a terrigenous saline basin, China: *Organic Geochemistry*, v. 11, p. 549–562, doi:10.1016/0146-6380(87)90009-X.
- Qin, Z., Zhi, D., and Xi, K., 2021, Organic petrology, geochemistry, and hydrocarbon generation capacity of Permo–Carboniferous source rocks in the Mahu Sag, northwestern Junggar Basin, China: *Energy Exploration & Exploitation*, p. 014459872110238, doi:10.1177/01445987211023856.
- Quan, T.M., Adigwe, E.N., Riedinger, N., and Puckette, J., 2013, Evaluating nitrogen isotopes as proxies for depositional environmental conditions in shales: Comparing Caney and Woodford Shales in the Arkoma Basin, Oklahoma: *Chemical Geology*, v. 360–361, p. 231–240, doi:10.1016/j.chemgeo.2013.10.017.
- Reich, P.B., and Oleksyn, J., 2004, Global patterns of plant leaf N and P in relation to temperature and latitude: *Proceedings of the National Academy of Sciences of the United States of America*, v. 101, p. 11001–11006, doi:10.1073/pnas.0403588101.

- Robinson, R.S. et al., 2012, A review of nitrogen isotopic alteration in marine sediments: *Paleoceanography*, v. 27, p. 2012, doi:10.1029/2012PA002321.
- Dos Santos, P.C., Fang, Z., Mason, S.W., Setubal, J.C., and Dixon, R., 2012, Distribution of nitrogen fixation and nitrogenase-like sequences amongst microbial genomes: *BMC Genomics*, v. 13, doi:10.1186/1471-2164-13-162.
- Sammy, N., 1983, Biological systems in north-western Australian solar salt fields. In: Schreiber, B.C., Harner, H.L. (Eds.), *Sixth Symposium on Salt*, vol. 1, The Salt Institute, Toronto, pp. 207–215.
- Schlacher, T.A., and Connolly, R.M., 2014, Effects of acid treatment on carbon and nitrogen stable isotope ratios in ecological samples: A review and synthesis: *Methods in Ecology and Evolution*, v. 5, p. 541–550, doi:10.1111/2041-210X.12183.
- Scott, C., and Lyons, T.W., 2012, Contrasting molybdenum cycling and isotopic properties in euxinic versus non-euxinic sediments and sedimentary rocks: Refining the paleoproxies: *Chemical Geology*, v. 324–325, p. 19–27, doi:10.1016/j.chemgeo.2012.05.012.
- Sigman, D.M., Karsh, K.L., and Casciotti, K.L., 2009, Nitrogen Isotopes in the Ocean, *in* Steele, J.H., Turekian, K.K., and Thorpe, S.A. eds., *Encyclopedia of Ocean Sciences*, 2nd ed., London, Academic Press, p. 40–54, doi:10.1016/B978-012374473-9.00632-9.
- Stüeken, E.E., Buick, R., Guy, B.M., and Koehler, M.C., 2015a, Isotopic evidence for biological nitrogen fixation by molybdenum-nitrogenase from 3.2 Gyr: *Nature*, v. 520, p. 666–669, doi:10.1038/nature14180.
- Stüeken, E.E., Buick, R., and Schauer, A.J., 2015b, Nitrogen isotope evidence for alkaline lakes on late Archean continents: *Earth and Planetary Science Letters*, v. 411, p. 1–10, doi:10.1016/j.epsl.2014.11.037.
- Stüeken, E.E., Kipp, M.A., Koehler, M.C., and Buick, R., 2016, The evolution of Earth's biogeochemical nitrogen cycle: *Earth-Science Reviews*, v. 160, p. 220–239, doi:10.1016/j.earscirev.2016.07.007.
- Stüeken, E.E., Martinez, A., Love, G., Olsen, P.E., Bates, S., and Lyons, T.W., 2019, Effects of pH on redox proxies in a Jurassic rift lake: Implications for interpreting environmental records in deep time: *Geochimica et Cosmochimica Acta*, v. 252, p. 240–267, doi:10.1016/j.gca.2019.03.014.
- Stüeken, E.E., Tino, C., Arp, G., Jung, D., and Lyons, T.W., 2020, Nitrogen isotope ratios trace high-pH conditions in a terrestrial Mars analog site: *Science advances*, v. 6, p. eaay3440, doi:10.1126/sciadv.aay3440.
- Talbot, M.R., 2001, Nitrogen Isotopes in Palaeolimnology, *in* W.M., L. and J.P., S. eds., *Tracking Environmental Change Using Lake Sediments*, Kluwer Academic Publishers, p. 401–439, doi:10.1007/0-306-47670-3_15.
- Talbot, M.R., and Johannessen, T., 1992, A high resolution palaeoclimatic record for the last 27,500 years in tropical West Africa from the carbon and nitrogen isotopic composition of lacustrine organic matter: *Earth and Planetary Science Letters*, v. 110, p. 23–37, doi:10.1016/0012-821X(92)90036-U.
- Tapia, J., Davenport, J., Townley, B., Dorador, C., Schneider, B., Tolorza, V., and von Tümpling, W., 2018, Sources, enrichment, and redistribution of As, Cd, Cu, Li, Mo, and

- Sb in the Northern Atacama Region, Chile: Implications for arid watersheds affected by mining: *Journal of Geochemical Exploration*, v. 185, p. 33–51, doi:10.1016/j.gexplo.2017.10.021.
- Tesdal, J.E., Galbraith, E.D., and Kienast, M., 2013, Nitrogen isotopes in bulk marine sediment: Linking seafloor observations with subseafloor records: *Biogeosciences*, v. 10, p. 101–118, doi:10.5194/bg-10-101-2013.
- Thomazo, C., and Papineau, D., 2013, Biogeochemical cycling of nitrogen on the early earth: *Elements*, v. 9, p. 345–351, doi:10.2113/gselements.9.5.345.
- Wang, X., He, S., Guo, X., Zhang, B., and Chen, X., 2018, The Resource Evaluation of Jurassic Shale in North Fuling Area, Eastern Sichuan Basin, China: *Energy and Fuels*, v. 32, p. 1213–1222, doi:10.1021/acs.energyfuels.7b03097.
- Warren, J.K., 2016, Halotolerant Life in Feast or Famine: Organic Sources of Hydrocarbons and Fixers of Metals, *in* *Evaporites*, Springer International Publishing, p. 833–958, doi:10.1007/978-3-319-13512-0_9.
- Warren, J.K., 1986, Shallow-water evaporitic environments and their source rock potential.: *Journal of Sedimentary Petrology*, v. 56, p. 442–454, doi:10.1306/212f8940-2b24-11d7-8648000102c1865d.
- Wartes, M.A., Carroll, A.R., and Greene, T.J., 2002, Permian sedimentary record of the Turpan-Hami basin and adjacent regions, northwest China: Constraints on postamalgamation tectonic evolution: *Bulletin of the Geological Society of America*, v. 114, p. 131–152, doi:10.1130/0016-7606(2002)114<0131:PSROTT>2.0.CO;2.
- Wei, W., and Algeo, T.J., 2019, Elemental proxies for paleosalinity analysis of ancient shales and mudrocks: *Geochimica et Cosmochimica Acta*, v. 287, p. 341–366, doi:10.1016/j.gca.2019.06.034.
- Wei, W., Algeo, T.J., Lu, Y., Lu, Y.C., Liu, H., Zhang, S., Peng, L., Zhang, J., and Chen, L., 2018, Identifying marine incursions into the Paleogene Bohai Bay Basin lake system in northeastern China: *International Journal of Coal Geology*, v. 200, p. 1–17, doi:10.1016/j.coal.2018.10.001.
- Xia, L., Cao, J., Hu, S., and Li, S., 2019a, How marine incursion influences the quality of lacustrine source rocks: The Paleogene Nanxiang Basin, eastern China: *AAPG Bulletin*, v. 103, p. 1071–1096, doi:10.1306/101261817268.
- Xia, L., Cao, J., Hu, S., Li, S., and Shi, C., 2019b, Organic geochemistry, petrology, and conventional and unconventional hydrocarbon resource potential of Paleogene saline source rocks in eastern China: The Biyang Sag of the Nanxiang Basin: *Marine and Petroleum Geology*, v. 101, p. 343–354, doi:10.1016/j.marpetgeo.2018.11.032.
- Xia, L., Cao, J., Hu, W., Zhi, D., Tang, Y., Li, E., and He, W., 2021a, Coupling of paleoenvironment and biogeochemistry of deep-time alkaline lakes: A lipid biomarker perspective: *Earth-Science Reviews*, v. 213, p. 103499, doi:10.1016/j.earscirev.2020.103499.
- Xia, L., Cao, J., Lee, C., Stüeken, E.E., Zhi, D., and Love, G.D., 2021b, A new constraint on the antiquity of ancient haloalkaliphilic green algae that flourished in a ca. 300 Ma Paleozoic lake: *Geobiology*, v. 19, p. 147–161, doi:10.1111/gbi.12423.

- Xia, L., Cao, J., Lee, C., Stüeken, E.E., Zhi, D., and Love, G.D., 2020a, A new constraint on the antiquity of ancient haloalkaliphilic green algae that flourished in a ca. 300 Ma Paleozoic lake: *Geobiology*, v. 19, p. 147–161, doi:10.1111/gbi.12423.
- Xia, L., Cao, J., Stüeken, E.E., Zhi, D., Wang, T., and Li, W., 2020b, Unsynchronized evolution of salinity and pH of a Permian alkaline lake influenced by hydrothermal fluids: A multi-proxy geochemical study: *Chemical Geology*, v. 541, p. 119581, doi:10.1016/j.chemgeo.2020.119581.
- Xu, W. et al., 2017, Carbon sequestration in an expanded lake system during the Toarcian oceanic anoxic event: *Nature Geoscience*, v. 10, p. 129–134, doi:10.1038/ngeo2871.
- Yang, J., Junium, C.K., Grassineau, N. V., Nisbet, E.G., Izon, G., Mettam, C., Martin, A., and Zerkle, A.L., 2019, Ammonium availability in the Late Archaean nitrogen cycle: *Nature Geoscience*, v. 12, p. 553–557, doi:10.1038/s41561-019-0371-1.

Figure and Table captions

Figure 1 Map showing the location and ages of the studied lacustrine sediments in China. (a) The location map. Mixed basins are referred to those with older marine sediments and younger lacustrine sediments, and the boundaries of marine and lacustrine sediments are distinct in different basins; (b) The stratigraphic figure showing the ages of samples.

Figure 2 Plots of (a) total nitrogen (TN) versus total organic carbon (TOC) contents of fresh-to-brackish samples, (b) TN versus TOC contents of brackish-to-saline, circum-neutral samples, (c) TN versus TOC contents of brackish-to-saline, alkaline samples, (d) total $\delta^{15}\text{N}$ versus C/N ratios, (e) organic carbon/total nitrogen (C/N) ratios versus TOC contents, and (f) organic carbon isotopes ($\delta^{13}\text{C}_{\text{org}}$) versus TOC contents. We lumped the other Formations from the Junggar Basin in one symbol for the readability, considering the relative similarity of geologic ages (compared with Jurassic and Eocene samples) and sedimentary conditions of other Formations from the Junggar Basin, including Carboniferous, the lower Permian Jiamuhe Formation, the middle Permian Pingdiquan and lower-Wuerhe Formations.

Figure 3 Plots of (a) carbonate carbon isotopes ($\delta^{13}\text{C}_{\text{carb}}$) versus oxygen isotopes ($\delta^{18}\text{O}_{\text{carb}}$), (b) Mn versus Sr, (c) $\delta^{13}\text{C}_{\text{carb}}$ versus total carbonate contents, and (d) $\delta^{18}\text{O}_{\text{carb}}$ versus total carbonate contents.

Figure 4 Relationship between salinity and $\delta^{15}\text{N}$ values. (a) $\delta^{15}\text{N}$ versus $\delta^{18}\text{O}_{\text{carb}}$; (b) $\delta^{15}\text{N}$ versus Sr/Ba; (c) $\delta^{15}\text{N}$ versus TOC/TS; (d) $\delta^{15}\text{N}$ versus B/Ga. Thresholds indicated by red dotted lines are taken from (Degens et al., 1957; Berner and Raiswell, 1984; Wei et al., 2018). The trend lines of the non-linear relationships are calculated by a widely-used graphics software named Origin 2021 with 95% confidence interval error bars (the blue shaded areas). Because all p-values in this figure are lower than 0.01, the correlations are believed to be reliable.

Figure 5 Reconstructed paleo-salinities of water mass during the deposition of lacustrine

sediments in this study. (a) $\delta^{18}\text{O}_{\text{carb}}$ versus Sr/Ba of C₂–P_{1f}; (b) TOC/TS versus Sr/Ba; (c) B/Ga versus Sr/Ba; (d) B/Ga versus TOC/TS. Thresholds indicated with red dotted lines are taken from (Degens et al., 1957; Berner and Raiswell, 1984; Wei et al., 2018). The trend lines were calculated as in Figure 4.

Figure 6 Nitrogen cycling during the deposition of lacustrine sediments in China. (a) Nitrogen cycling of circum-neutral Groups 1 and 2; (b) Nitrogen cycling of alkaline Group 3 (adapted from Collister and Hays, 1973). Fractionations are defined as $\varepsilon \approx \delta^{15}\text{N}_{\text{product}} - \delta^{15}\text{N}_{\text{reactant}}$. Isotopic fractionations are from literatures (Casciotti, 2009; Godfrey and Glass, 2011; Li et al., 2012; Brunner et al., 2013; Stüeken et al., 2015a, 2016; Deng et al., 2018).

Figure 7 $\delta^{15}\text{N}$ values, C/N ratios, and $\delta^{13}\text{C}_{\text{org}}$ values in circum-neutral fresh-to-brackish Group 1 and brackish-to-saline Group 2. (a) $\delta^{15}\text{N}$ versus C/N of Group 1; (b) $\delta^{15}\text{N}$ versus $\delta^{13}\text{C}_{\text{org}}$ of Group 1; (c) $\delta^{15}\text{N}$ versus C/N of Group 2; (d) $\delta^{15}\text{N}$ versus $\delta^{13}\text{C}_{\text{org}}$ of Group 2. Because Figure 7 is for one possible explanation to the co-variation between salinity and $\delta^{15}\text{N}$ value in circum-neutral groups, data of alkaline Group 3 are not shown in Figure 7. The trend lines were calculated as in Figure 4.

Figure 8 Redox conditions during deposition of the studied lacustrine sediments and their correlation with salinities. (a) Mo content versus U/Th; (b) Correlation between O₂ content and salinity (modified after Javor, 1983, 1985; Mitchell and Geddes, 1977; Sammy, 1985; Warren, 1986); (c) TOC/TS versus Mo content; (d) Sr/Ba versus Mo content. The trend lines were calculated as in Figure 4.

Figure 9 Effects of salinity and redox state on $\delta^{15}\text{N}$ values. (a) $\delta^{15}\text{N}$ versus salinity from $\delta^{18}\text{O}_{\text{carb}}$ (alkaline group); (b) $\delta^{15}\text{N}$ versus salinity from TOC/TS (circum-neutral group); (c) $\delta^{15}\text{N}$ versus redox state from Mo content (alkaline group); (d) $\delta^{15}\text{N}$ versus redox state from Mo content (circum-neutral group). The trend lines were calculated as in Figure 4.

Table 1 List of samples analyzed in this study. No = sample number. Depth is in meters. E_{2s3} = third member of E_{2s}; E_{2s4} = fourth member of E_{2s}; E_{2q3} = third member of E_{2q}; E_{2q4} = fourth member of E_{2q}; E_{2h3} = third member of E_{2h}; E_{2s1} = first member of E_{2s}.

Table 2 The synthesis of sedimentary environments from Carboniferous–Paleogene lacustrine basins in China (Philp and Fan, 1987; Cao et al., 2005; Xu et al., 2017; Wei et al., 2018; Li et al., 2018; Liu et al., 2019; Xia et al., 2019b; Cao et al., 2020).

Figure 1

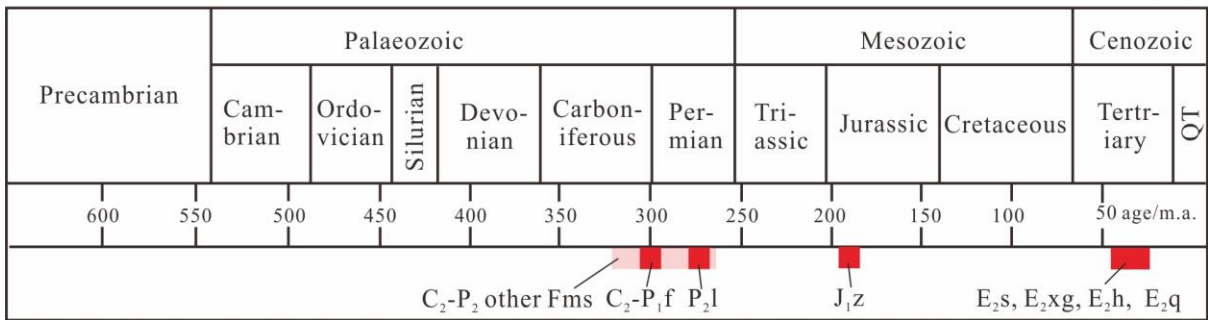
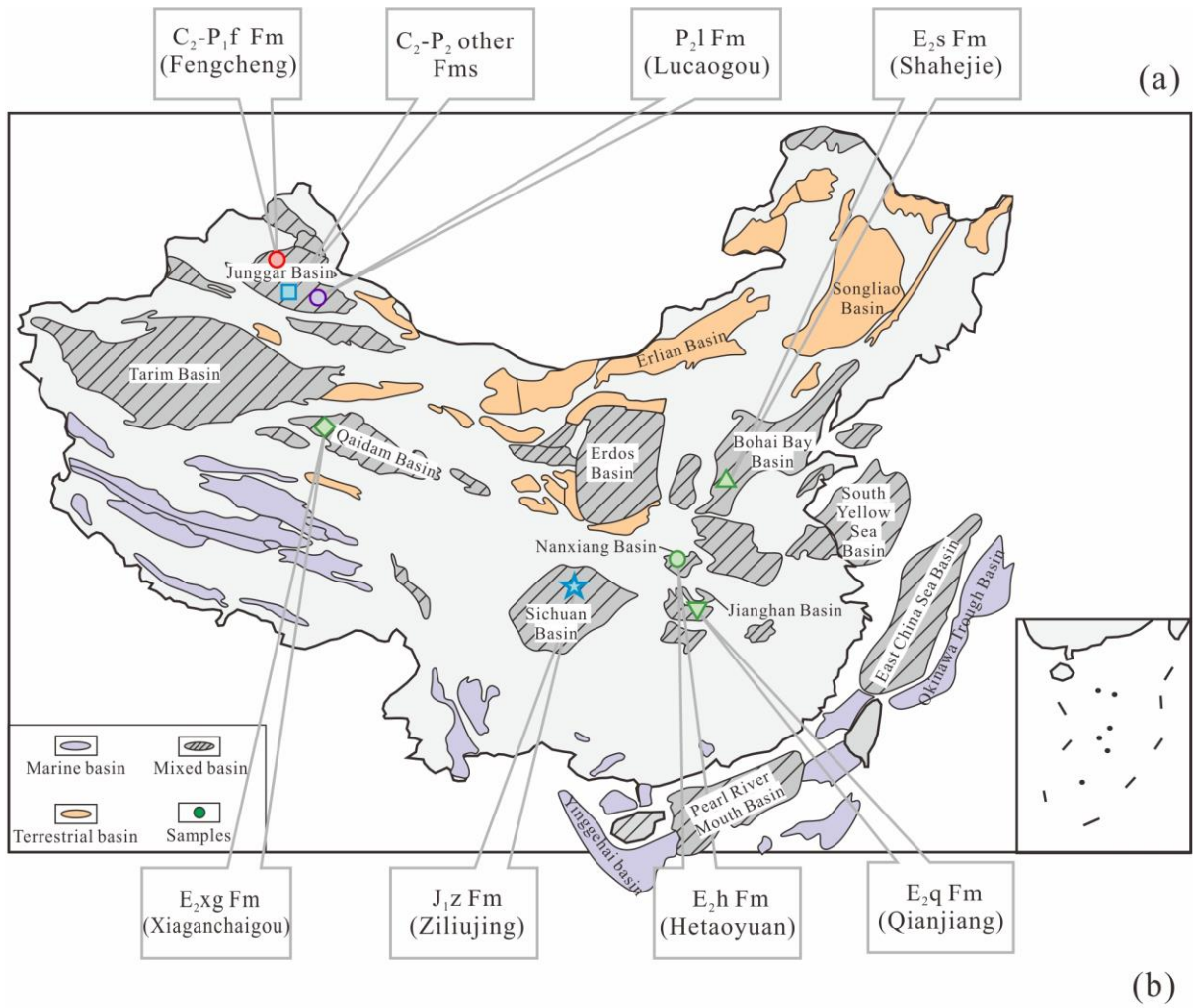


Figure 2

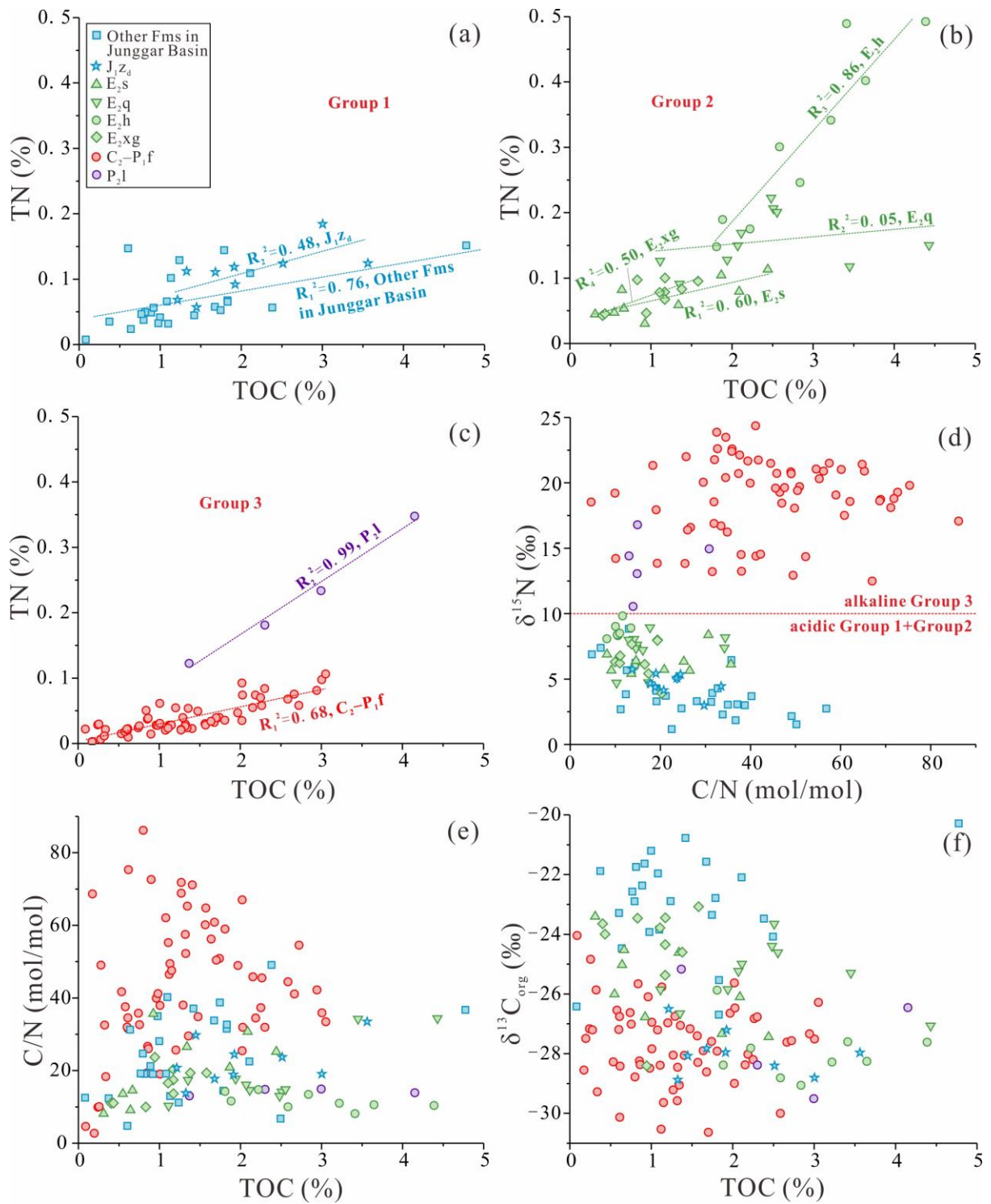


Figure 3

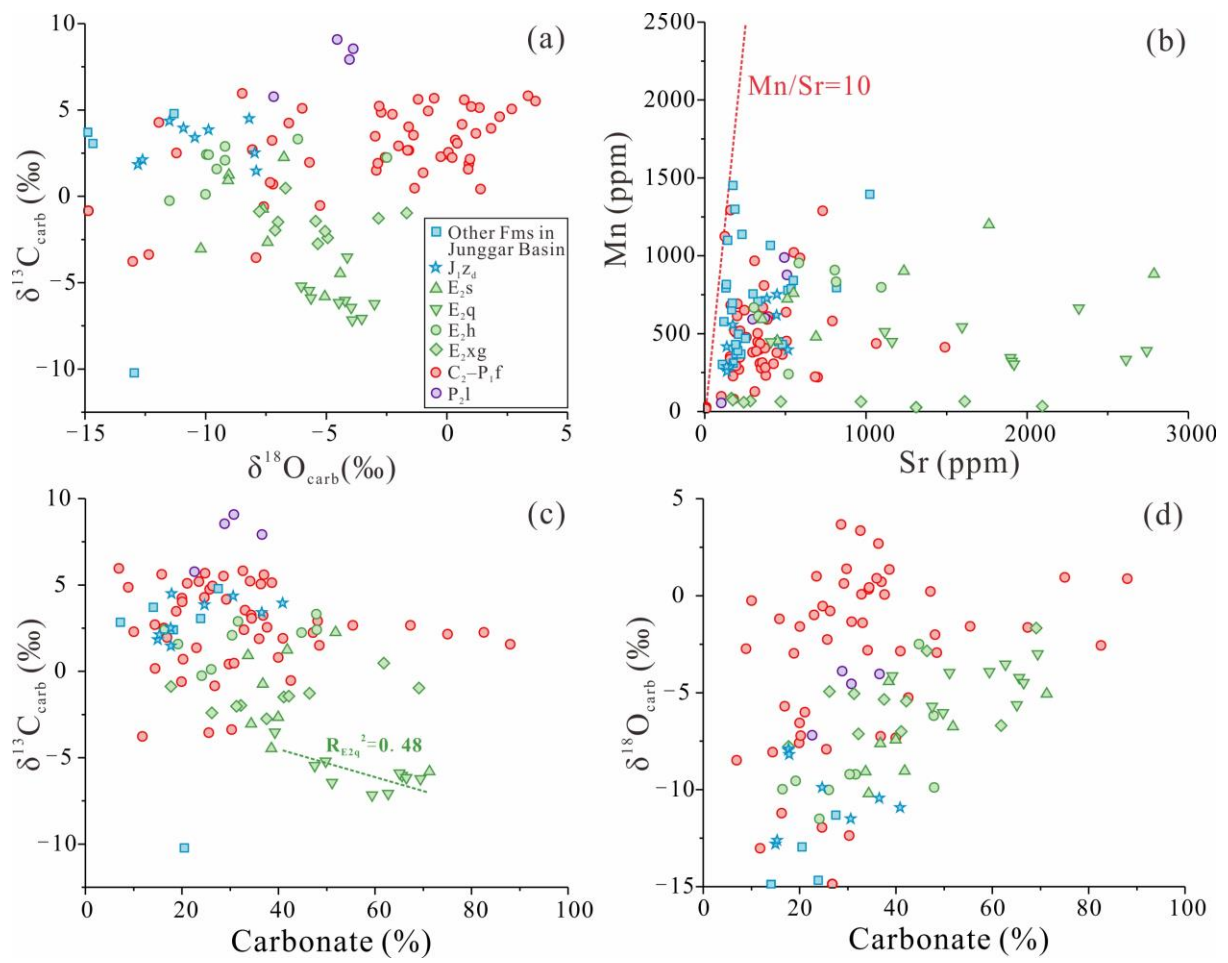


Figure 4

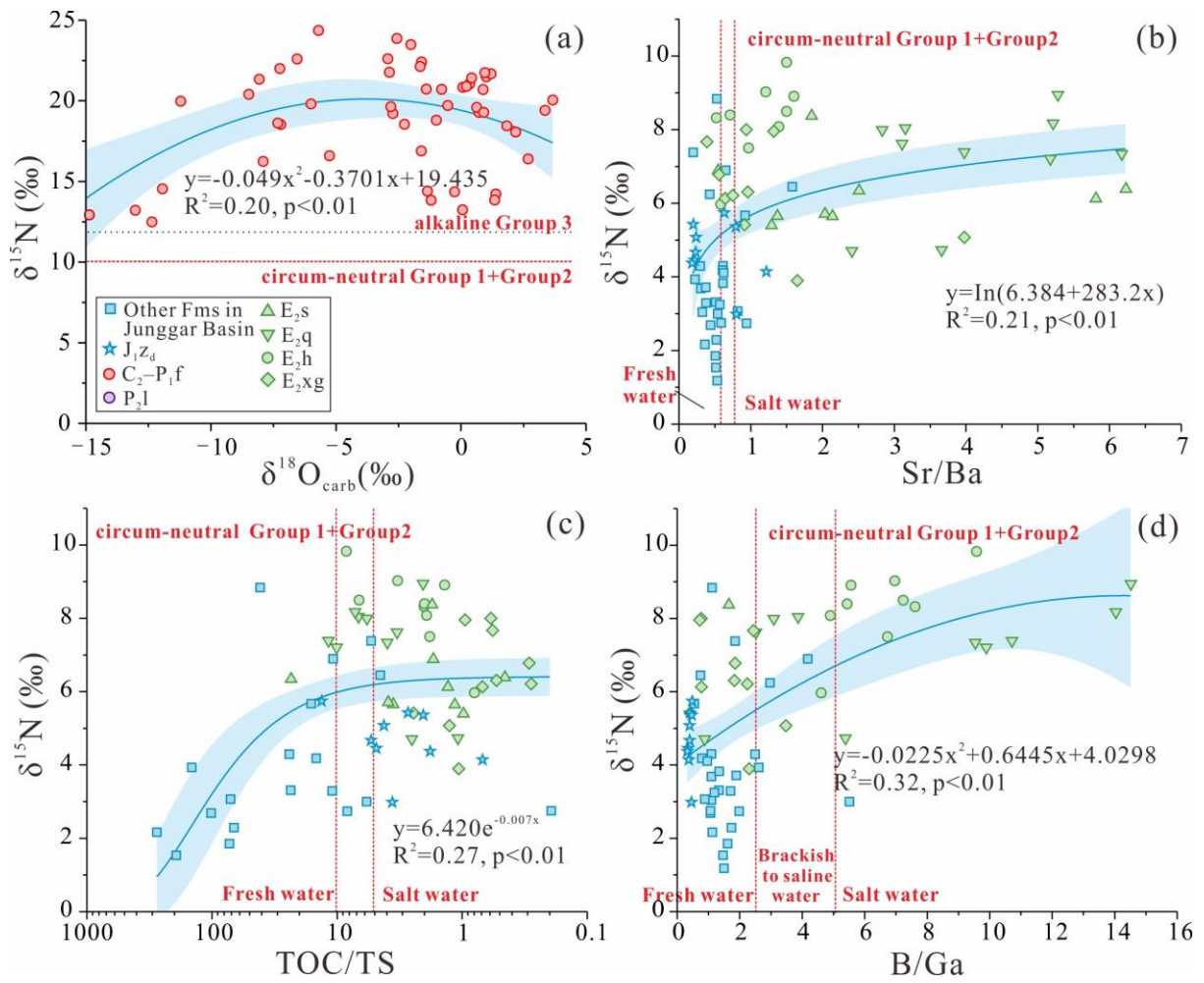


Figure 5

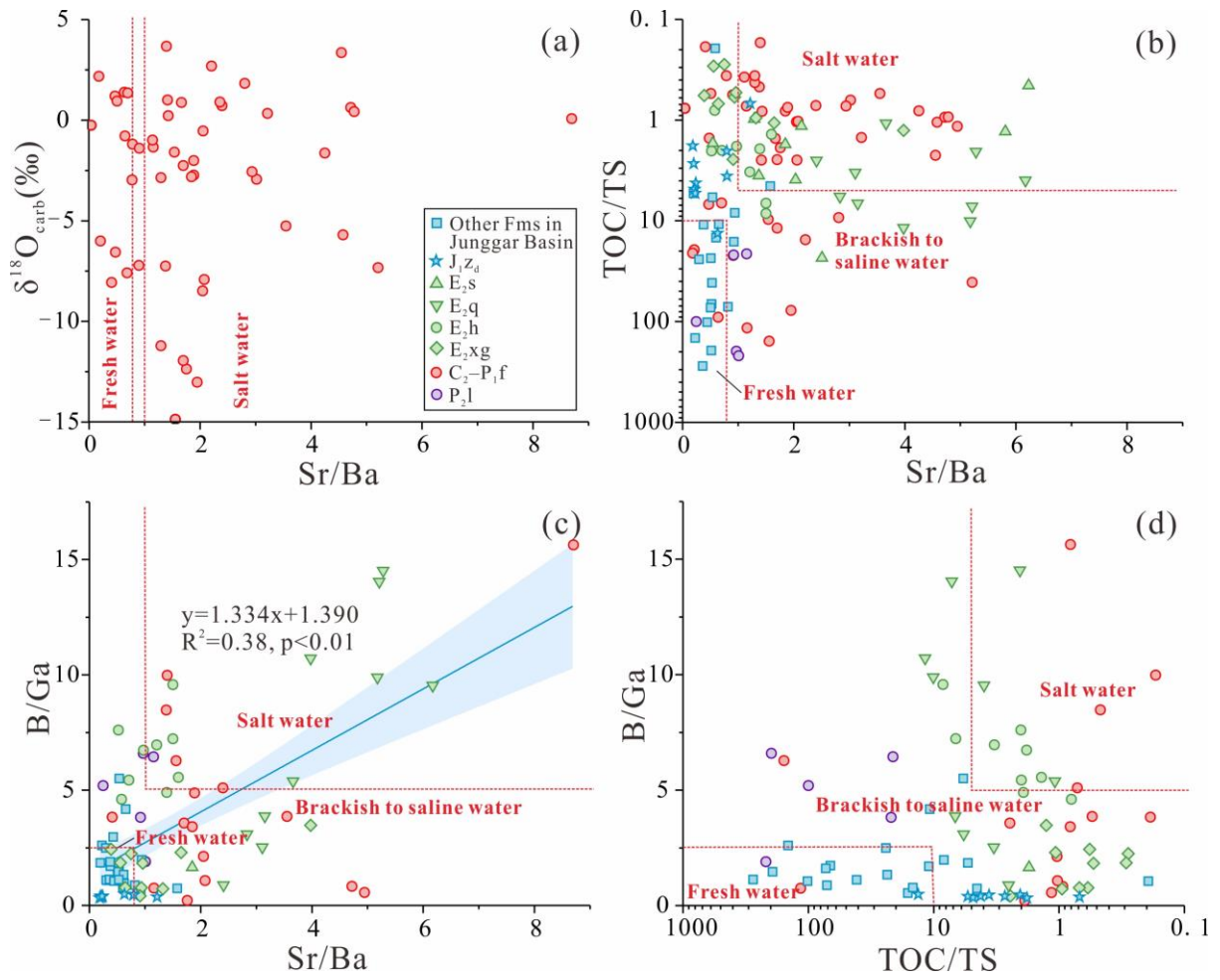


Figure 6

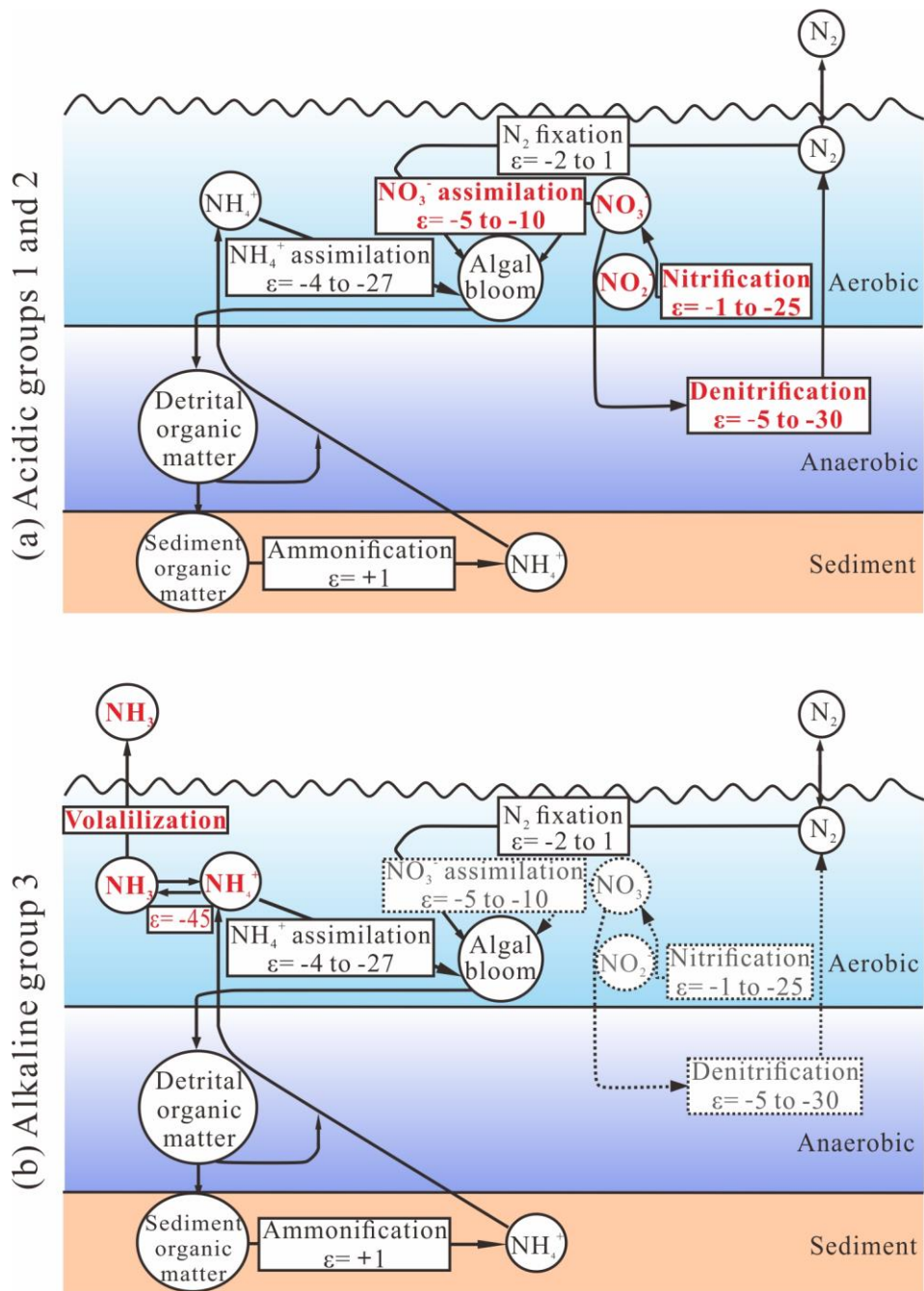


Figure 7

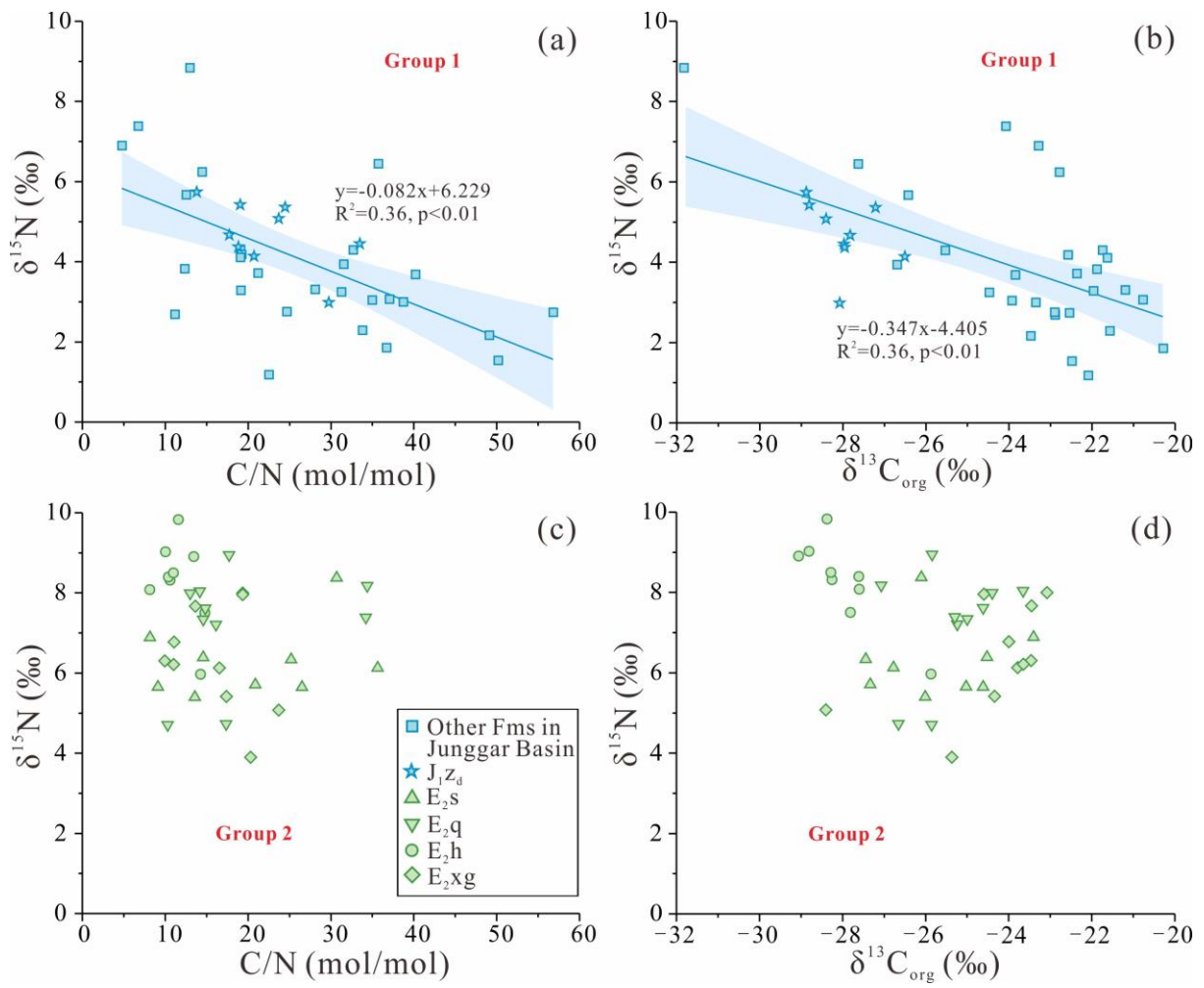


Figure 8

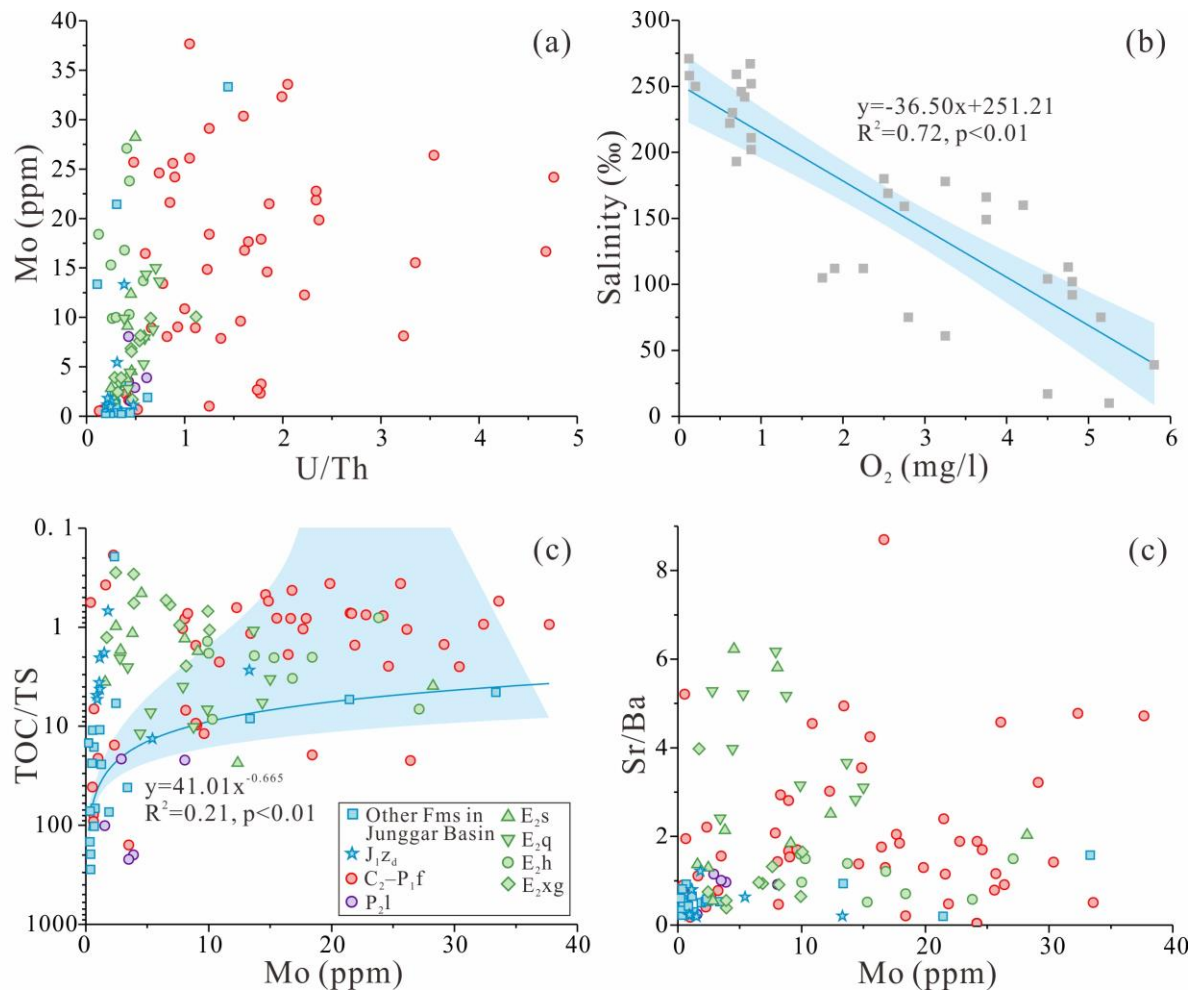


Figure 9

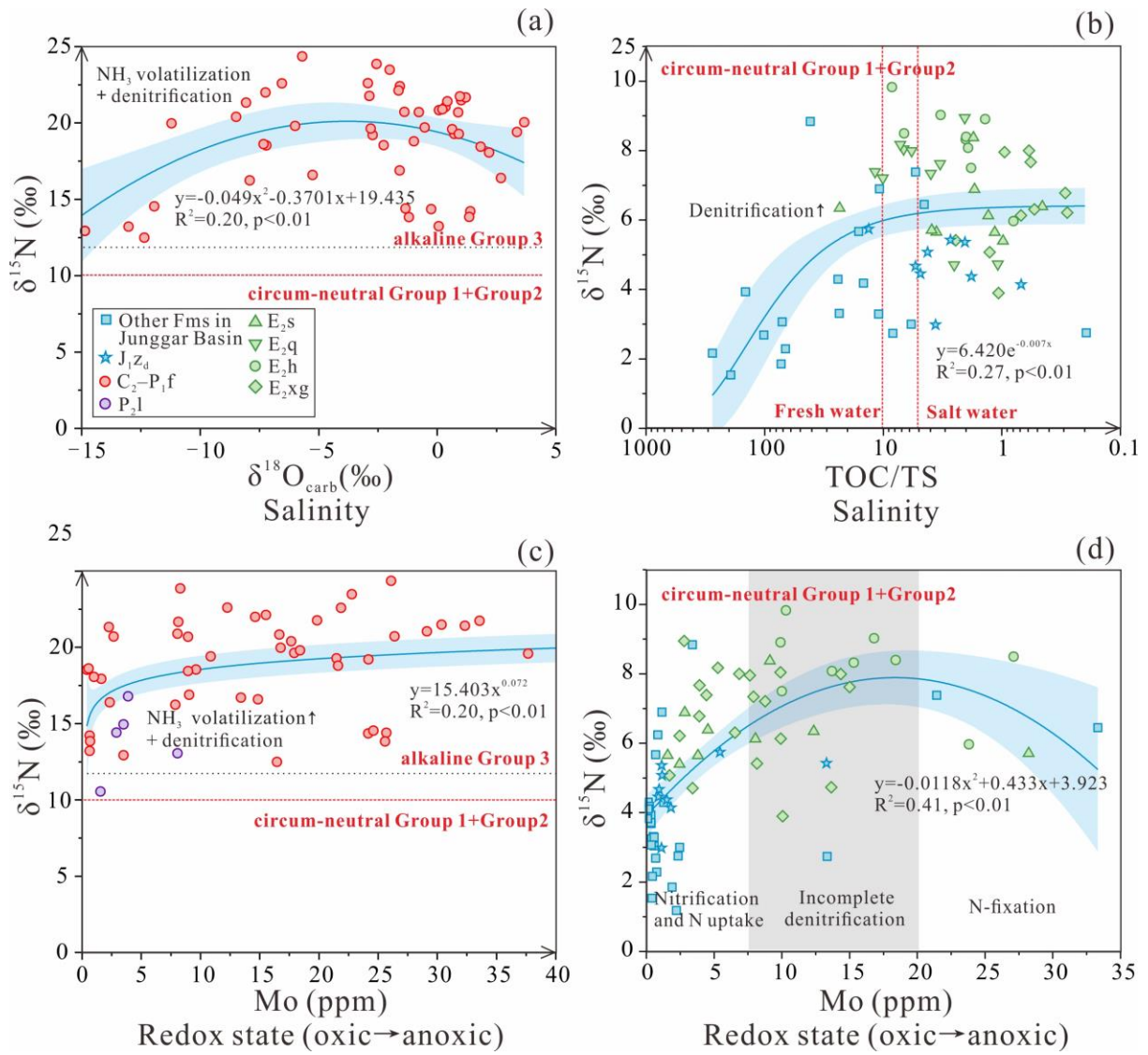


Table 1

No.	Location	Core	Stratum	Depth (m)	No.	Location	Core	Stratum	Depth (m)
1	Mahu Sag, Junggar Basin	Xia87	C ₂ -P ₁ f ₁	4154	74	Junggar Basin	Ke85	C ₂ j	3419.2
2		Xia76	C ₂ -P ₁ f ₃	3455.5	75		Guai16		2813.1
3			C ₂ -P ₁ f ₁	3645.6	76				2813.7
4		X40	C ₂ -P ₁ f ₃	4577.7	77				2814.3
5				4578.5	78				2814.8
6				4581.5	79		Guai15		2807.3

7			C ₂ -P ₁ f ₂	4638.4	80		F3		1151.2
8			C ₂ -P ₁ f ₂	4764.5	81		F3		1152.9
9		W351	C ₂ -P ₁ f ₃	3316.2	82				3066.1
10		FN8	C ₂ -P ₁ f ₃	3595	83		Xia40		3479.0
11			C ₂ -P ₁ f ₃	4340	84				3479.7
12			C ₂ -P ₁ f ₃	4360	85		Ke76	P ₂ w	2965.8
13				4440	86				2967.3
14				4590.8	87				3590.6
15				4591	88		Ma004		3596.81
16				4592	89				3603.6
17				4595	90				3637.5
18			C ₂ -P ₁ f ₂	4596.2	91				4358.4
19				4598.5	92		AS1		4574.2
20				4640	93				4629.8
21				4700	94				5048.9
22				4880	95				
23				4065.5	96				2276.5
24				4066.3	97		SS1	P ₂ p	2317
25		FN5	C ₂ -P ₁ f ₂	4068.9	98				2375
26				4069	99				2400.9
27				4071	100				2406.3
28				4065.2	101		Lian16		3342.7
29				4082.3	102		Xi20		2773.0
30				4095	103		Xi28		2779.1
31				4112.6	104		Xiao3		2788
32		FN14	C ₂ -P ₁ f ₃	4166.8	105	Central Sichuan Basin	Xi20	J ₁ zd	2801.8
33			C ₂ -P ₁ f ₂	4096.5	106		Xiang3		2805.6
34				4238.4	107		Gong4		2808.8
35		FN1	C ₂ -P ₁ f ₂	4341.8	108		Shi3		2821.3
36				4423.1	109		Wen11		2824.7
37			C ₂ -P ₁ f ₁	4450.6	110		Wen14	E ₂ s ₁	2533.1
38		FC1	C ₂ -P ₁ f ₁	3900	111	Dongpu Sag, Bohai	Wen33- Wen17	E ₂ s ₃	3060.6
39				3990	112		Wen24		3053.2
40				4010	113		Wei79-	E ₂ s ₄	3388.5
41				3194.4	114	Bay Basin	Qiao17		3429.8
42			C ₂ -P ₁ f ₃	3220.8	115			E ₂ s ₃	3647.7
43			C ₂ -P ₁ f ₂	3250	116		Ma11-7		2755.8
44				3437	117			E ₂ s ₄	3316.7
45				3138.3	118		Hao87		3403.5
46				3139.1	119		Zhou26	E ₂ q ₄	2588.7
47				3151.3	120				2845.8
48				3152.3	121	Qianjiang Sag, Jiangnan Basin			1770.1
49			C ₂ -P ₁ f ₃	3162	122		W4X-7	E ₂ q ₃	1771.9
50				3187.9	123		-7		1772
51				3188.8	124				1772.9
52				3248	125				1773.5
53				3248.8	126				1773.9
54				3250.5	127				1775.0
									1776

55				3251.1	128	Biyang Sag, Nanxiang Basin	An3006	E _{2h3}	3342.7
56				3268.0	129				2773.0
57				3269.1	130				2779.1
58		BQ1	C ₂ -P _{1f2}	4103	131				2788
59		Bai26	C ₂ -P _{1f3}	3360	132				2801.8
60			C ₂ -P _{1f2}	3811	133				2805.6
61		AK1	C ₂ -P _{1f1}	5661.5	134				2808.8
62				5662	135				2821.3
63				5663	136				2824.7
64				5664.3	137				3849.4
65				5665.9	138				3850.9
66				5668	139				3854.3
67	Jimusaer Sag, Junggar Basin	J174	P _{2l}	3133	140				Western Qaidam Basin
68		J174		3194.5	141	3865.9			
69		J174		3213.5	142	3866.9			
70		J174		3276.4	143	4486.8			
71		J36		4213.5	144	4488.8			
72		HG5	C _{2j}	2960	145	Shi203			4499
73		Ke85	C _{2j}	3416.2	146				4502.5

Table 2

Location	Stratum	Group	TOC (wt.)	$\delta^{13}\text{C}_{\text{org}}$ (‰)	$\delta^{15}\text{N}$ (‰)	Salinity	Redox state
Juggar Basin	C ₂ , C _{2j} , P _{2W} , P _{2p}	Group 1 (fresh-to-brackish circum-neutral)	0.4–12.4	-27.6– -20.3	1.2– 8.8	Fresh to brackish	Oxic to anoxic
Middle Sichuan Basin	J _{1zd}		1.2–3.6	-28.9– -26.5	3.0– 5.7	Fresh to brackish	Oxic to suboxic
Dongpu Sag, Bohai Bay Basin	E _{2s}	Group 2 (brackish-to-saline circum-neutral)	0.3–2.4	-27.4– -23.4	5.4– 8.4	Saline to saltwater	Suboxic–anoxic
Qianjiang Sag, Jiangnan Basin	E _{2q}		1.1–4.4	-27.1– -23.7	4.7– 8.9	Saline to saltwater	Suboxic–anoxic
Biyang Sag, Nanxiang Basin	E _{2h3}		1.8–4.4	-29.1– -25.9	6.0– 9.8	Brackish to saltwater	Suboxic–anoxic
Western Qaidam Basin	E _{2xg}		0.4–1.6	-28.4– -23.1	3.9– 8.0	Brackish to saltwater	Suboxic–anoxic
Mahu Sag,	C ₂ -P _{1f}		Group 3	0.2–3.1	-30.6–	10.1–	Saline to

Juggar Basin		(ackish-to		-24.0	24.4	saltwater	anoxic
Jimusaer Sag, Juggar Basin	P ₂ l	saline alkaline)	1.4-7.8	-29.5- -25.2	10.6- 16.8	Brackish to saltwater	Suboxic to anoxic